Frictional behaviour of halite/muscovite fault gouge analogues: Effects of sliding velocity and of stepwise acceleration from sub- to co-seismic slip rates

MSc Thesis A.J.L. Buijze, 0476609, Utrecht University

29 November 2010

Abstract

Investigating the (transient) frictional behaviour of fault rock from low to high velocities is required in experimental research on the stability of faults and earthquake behaviour. Fault stability is an important factor controlling earthquake nucleaction, and it may also control the subsequent propagation of rupture over the fault zone. Rupture may propagate easily in unstable fault rock, but may be inhibited by a stably deforming region (eg.a region deforming by creep). Also phyllosilicates are ubiquitous in natural fault rock and may influence deformation behaviour. Experiments on analogue gouge were conducted in the low-to-high-velocity rotary shear apparatus (HV2 machine) at Hiroshima University. Both pure halite and halite + muscovite were sheared from 0.1 μms^{-1} up to 1 ms^{-1} at room-dry conditions and a low normal stress (5MPa). Mechanical data and microstructural evidence reveal velocity weakening from 1 μms^{-1} to ~0.01 ms^{-1}, deformation being brittle and very localized, velocity strengthening from 0.01-0.1 ms^{-1} with deformation by an interplay of the formation of strong dense aggregates by healing and breaking up this material in smaller fragments in a distributed manner, and strong velocity weakening from 0.1-1 ms^{-1}, where strong localization and possibly melting occur. Pressure solution occurs to some extent in the room-dry gouges, presumably causing observed stick-slip behaviour and healing. The addition of muscovite causes a lower frictional strength and more unstable behaviour from 0.1-10 μms^{-1}, and is slightly higher velocity strengthening at 0.1 ms^{-1}. Wet halite + muscovite experiments conducted by Niemeijer & Spiers (2005) were reproduced in the HV2 machine from 0.01 μms^{-1} and extended to higher velocities, up to 0.1 ms^{-1} where pore water evaporates. At low velocities (< 1 μms^{-1}) the material is velocity strengthening, and sigmoidal halite clasts with the beginning of a muscovite foliation wrapping around them were observed. Velocity weakening was observed at velocities >1 μms^{-1}, with the microstructure revealing a cataclasic, well mixed structure with a zone where fine grained material has accumulated. The frictional behaviour was also found to depend on the surface roughness of the wall-rock; smoother wall-rock yields more loaclization and unstable behaviour. To simulate rupture coming in on the stably sliding zone, large velocity steps were conducted from this regime to higher velocities. These steps could be modelled with RSF. The velocity strengthening regime found in the room-dry experiments at 0.01-0.1 ms^{-1} may act as a barrier to earthquake rupture. To investigate this, several large velocity steps were made from the velocity strengthening regime into the high velocity regime, revealing an initial slip strengthening stage over a significant displacement, before a transition to rapid slip weakening occurred. This strengthening stage is not recognized in traditional rate-and-state friction (RSF), implying frictional behaviour is governed by different constitutive properties and extrapolation from RSF to the high-velocity regime may not be straightforward.

1. Introduction

Laboratory experiments investigating the stability and behaviour of rocks and fault gouges provide a rational means of improving our understanding of processes operating in natural faults (Dieterich, 1979). One of the main goals of experimental studies on rocks is to gain an understanding of the processes that govern earthquake behaviour. The frictional properties of rocks and fault gouges at slow slip rates and small displacements have been investigated in great detail and have lead to the development of constitutive relations that (quite successfully) describe fault strength in terms of slip rate and slip history; the so called rate-and-state constitutive equations (Dieterich, 1979; Ruina, 1983). These constitutive relation can be used in earthquake modelling and they are also important for crustal stress models, as fault strength may actually control crustal strength (Marone, 1998). High-velocity studies have been conducted since the late 1980s, and a lot of new insight into deformation mechanisms operating at these slip rates has been gained, but still not much is known about the constitutive properties at seismic slip rates. The earthquake cycle involves a broad range of slip rates, so understanding the frictional properties and the underlying deformation mechanisms over a large range of slip rates and large displacements is essential (Mizoguchi et al., 2009). Also the transient behaviour is important; what does actually happen as a rupture front passes and a fault is subject to accelerating and decelerating motion? The velocity dependence of the fault rock may vary with depth; earthquakes may nucleate in an unstable (velocity weakening) zone, but propagate into a stable (strengthening) zone. What happens when the rupture propagates into such a stably deforming zone?

Most studies have thus far focused on either low or high slip rates, and connections between the two regimes are generally lacking. In this study, we present results on analogue halite gouge exploring jumps from low to high velocities. Halite is often used to simulate natural quartzitic fault rocks because it exhibits brittle to plastic deformation behaviour at room temperatures and relatively low pressures, and the resulting microstructures resemble those found in nature (eg. Niemeijer & Spiers, 2005). Solution transfer processes are also fast at these conditions, making it a good analogue to study brittle-ductile deformation where cataclasis in combination with pressure solution is thought to operate. Many friction experiments on halite gouges have been conducted on (room) dry halite and have thus not investigated effects of pressure solution. Previous results on room-dry halite show that at 10 MPa, room temperature and slow slip rates halite behaves in a fully brittle manner, and upon increasing the pressure, a transition to fully plastic flow is observed from 30 to 250 MPa (Shimamoto & Logan, 1986). The halite exhibits unstable behaviour and becomes weaker with increasing velocity (velocity weakening) up to 1 μms^{-1}, after which it strengthens again up to 300

μms^{-1} (velocity strengthening). A recent study at low normal stresses (<10 MPa) and velocities approaching natural seismic velocities (0.02-1 ms^{-1}) reveal extreme weakening, accompanied by the formation of melt in the thin localized layer and heating induced plastic behaviour in a broader zone, deforming at a low slip rate, surrounding this melt zone (Kim et al., 2010).

Natural fault rocks mostly contain a large amount of phyllosilicates and are subject to hydrothermal conditions. This fact motivated a study on their influence on the behaviour of crustal fault strength by Bos et al. (2000a, 2000b), Bos & Spiers (2000, 2001, 2002, 2002b), Niemeijer & Spiers (2005, 2006, 2007). They conducted experiments under wet conditions at low velocities (0.001 – 10 μms^{-1}) on mixed halite-muscovite gouges. They find velocity strengthening (stable) behaviour at velocities less than 1 μms^{-1}. Microstructures revealed the formation of a mica-foliation wrapping around the halite clasts at those velocities, resembling very much natural fault rock structures found at the base of the seismogenic zone (eg. those found in the Shimanto belt, Japan). The authors interpreted deformation to occur by sliding of the halite clasts over the foliation, accommodated by pressure solution (frictional-viscous behaviour). At velocities higher than 1 μms^{-1} they find unstable behaviour and strong velocity weakening, and they propose this behaviour to involve a competition between dilatation caused by granular flow and compaction by pressure solution at the grain contacts. The higher the sliding velocity, the more net dilatation occurs and the higher the porosity.

In this study, we investigate the frictional properties and deformation mechanisms of analogue halite gouge over a wide range of velocities (0.1 μms^{-1} to 1 ms^{-1}) by reproducing and extending the analogue fault gouge studies conducted by Niemeijer & Spiers (2005) to higher velocities. Both pure halite and halite + muscovite gouges are analyzed at room-dry conditions, and at wet conditions halite + muscovite is studied.

Numerous studies have investigated the stability of fault gouges and have subsequently been successfully used in earthquake analysis. However, as mentioned earlier the transient portion of earthquake rupture, and the influence of the fault rock velocity dependence on this, are less well known. This study aims to simulate an earthquake rupture propagating into a velocity strengthening region, such as may exist at the bottom of the seismogenic zone. This is done by making a velocity jump of a few orders of magnitude from the frictional-viscous (strengthening) regime found by Niemeijer & Spiers (2005) into the velocity weakening regime at higher velocities.

1.1. Rate-and-state friction

Laboratory studies at low slip rates have given rise to the development of constitutive laws describing the frictional behaviour in terms of displacement, sliding velocity and the history of the slip surface. Frictional stability is a system response determined by the contact surface between 2 rocks masses (asperities) and their elastic surroundings (Marone, 1998). A friction constitutive model must take into account the observation that friction depends on both the loading rate and the slip history (Paterson & Wong, 2005). Under this assumption Dieterich (1979) and Ruina (1983) developed a rate- and state- dependent friction model. In this rate- and state- friction (RSF) model, friction is characterized by a friction law (which gives the frictional strength as a function of the sliding velocity and the 'state', or history, of the sliding surface) and an evolution law (which describes how the state of the sliding surface varies with time or slip). The friction law is given by

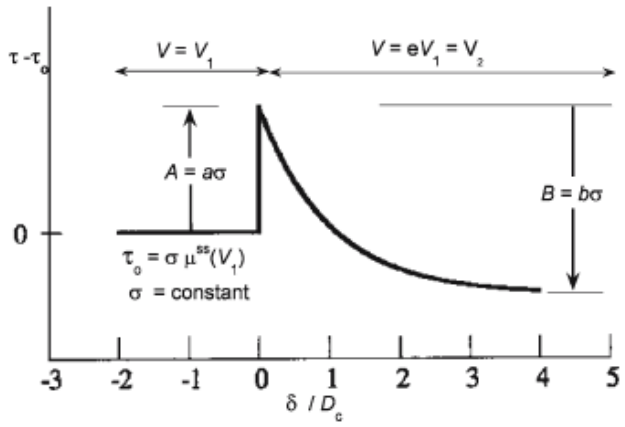

Figure 1 Typical behaviour expected from rate and state friction in case of an upstep in velocity by a factor of e. (2.701), illustrating how constitutive parameters can be determine, The direct effect is related to the velocity step by A($\ln V_1/V_2$) and the constitutive parameter B is related to the state effect. D_c is the characteristic slip weakening distance, corresponding to a decay in μ of 1/e. If a-b is positive, the system is velocity strengthening, if a-b is negative it is conditionally velocity weakening, depending on the machine stiffness.. (Paterson & Wong, 2005)

$$\mu = \mu^* + a \ln \frac{V}{V^*} + b \ln \frac{V^* \theta}{D_c} \tag{1}$$

where μ is the coefficient of friction (shear strength τ over the normal stress σ_n), V^* is the reference sliding velocity, V is the new velocity, μ^* the corresponding reference coefficient of friction, μ the new coefficient of friction, θ the state variable and D_c the characteristic sliding distance to steady state. The two dimensionless parameters $a=A/\sigma$ and $b=B/\sigma$ are related to respectively the 'direct effect', and the 'evolution effect'. Upon a change in sliding velocity there will be an instantaneous change in velocity proportional to the velocity change, which can be described by the rate-dependent term $Aln(V/V^*)$, where A is a constitutive parameter with the dimension of stress. B (also dimensions of stress) is a second constitutive parameter related to the evolution effect, describing how strength evolves after the direct effect.

There are two main evolution laws; a slip law (Ruina, 1983) and a slowness law (Dieterich, 1979). The slip law and slowness laws are expressed respectively as

$$\frac{d\theta}{dt} = -\frac{V\theta}{D_c} \ln \frac{V\theta}{D_c} \tag{2}$$

$$\frac{d\theta}{dt} = 1 - \frac{V\theta}{D_c} \tag{3}$$

Usually both laws fit velocity stepping data equally well. Inserting them into (1) the equation for a steady state frictional coefficient leads to

$$\mu_{ss} = \mu^* + (a-b) \ln \frac{V}{V^*} \tag{4}$$

To find values for a and b, inverse modelling of the data is

required. However, (a-b) can be read directly from the experimental data (see figure 1), and provides a measure of the velocity dependence, and thus the stability of a material. When a-b > 0, the system is velocity strengthening and when a-b < 0 , the system is conditionally unstable depending on the stiffness of the deformation apparatus.

1.2 High-velocity friction

At high velocities processes other than frictional ones start operating and the empirically determined RSF which works well at slow slip rates does not seem to apply anymore. We will briefly summarize the most important amongst them discovered in high velocity friction experiments. In 1994 frictional properties of simulated faults were first measured in a high-velocity testing machine (Tsutumi & Shimamoto, 1996), and since then our knowledge about frictional properties has increased greatly. Despite the progress made high-velocity experiments still remain challenging. The normal load that can be applied is very low due to the effect of thermal fracturing (Ohtomo & Shimamoto, 1994). Applying, measuring and controlling the pore fluid pressure is yet another unsolved problem, so the road to more in-situ conditions is still a long one. However, interesting theories resulted from the numerous high-velocity studies performed to date, especially over the last 15 years.

Multiple studies record extreme slip weakening and velocity weakening of simulated faults and fault gouges at seismic slip rates ~0.1-1 ms^{-1} (eg. Tsutumi & Shimamoto, 1997, Kim et al., 2010) and various mechanisms have been proposed to explain this weakening. Experiments investigating the frictional evolution with slip distance, associated with the formation of melt (Tsutumi and Shimamoto (1997), Hirose and Shimamoto (2005), Di Toro (2006), Del Gaudio (2009)), all show a first peak in strength to overcome static friction, followed by slip weakening, after which slip strengthening occurs to form a second peak, followed by slip weakening to very low frictional strengths. The first weakening may be caused by flash heating of asperity contacts. The contacts will undergo a local transient rise of temperature due to frictional heating, which is higher than the average temperature over the sliding surface. The local shear strength will presumably drop with this flash heating, therefore weakening the frictional strength of the material (Rice, 2006). Microstructural observation link the second weakening stage to the development of a through-going layer of melt , whereas the strengthening preceding this 'melt lubrication' reflects the formation and shearing of isolated high viscosity melt patches. Upon cooling during the experiment these may weld the fault surfaces together and strengthen the material.

Thermal pressurization is which is proposed as a slip weakening mechanism in earthquake generation (Sibson (1973), Wibberley and Shimamoto (2005), Rice (2006)). During rapid slip frictional heating occurs, the pore-fluid is heated and expands faster than the surrounding rock, leading to over pressurization, lowering of the effective normal stress and thus results in weakening of the material. High temperatures due to frictional heating may also lead to the decomposition of the rock or gouge material, which may in turn lead to weakening. This is for example seen in calcite gouges (Han et al., 2010) and kaolinite-bearing fault gouge (Brantut et al., 2008). Di Toro et al. (2004) propose the formation of silica-gel at grain contact as a weakening mechanism in quartz-rich rocks. The variety of hypotheses indicates that the last word has not been spoken on this topic. The newest studies start now focusing on accelerating and decelerating slip behaviour which is more like a natural earthquake (Sone & Shimamoto, 2009; Togo et al., 2009; Sawai, unpublished 2010).

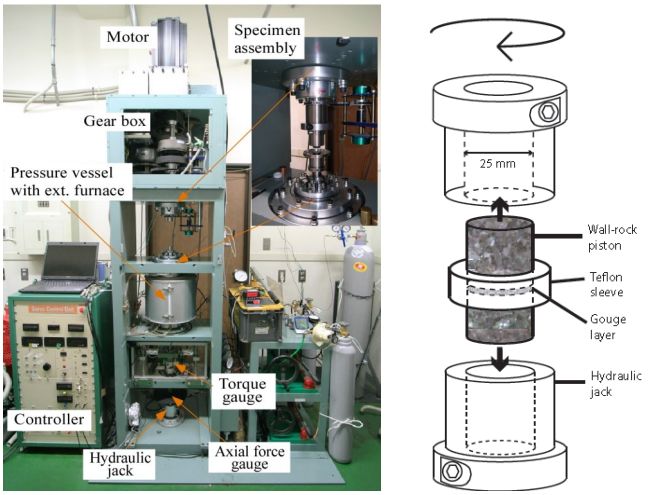

Figure 2 a) Photograph of the HV2 machine in Hiroshima University. The servomotor is located at the top of the machine, just above the gearbox which has 4 different gears. Normal load is applied via the bottom shaft (stationary shaft) by a gas cushioning system. The controller receives all the signal and sends them to the computer so data can be observed real time. b) Schematic drawing of the specimen assemhly used in this study. The wall-rock pistons can be connected to the rotary and stationary shaft by the hydraulic jacks.

2 Methods

2.1 Apparatus

Friction experiments were conducted at Hiroshima University in the 2d low-to-high velocity rotary shear testing apparatus (hereafter referred to as HV2 machine). A photograph of the HV2 machine is shown in figure 2a. Sliding velocity is controlled by a servo motor and a gear-and-belt system (top of diagram) driving a vertical rotary column. To create a wide range of velocities, there are 4 different gears named line 1-4 in the gear assembly, which can be switched by turning on and off an electromagnetic clutch. By the use of these gears, velocities from 3 mm/yr (~10^{-10} ms^{-1}) up to seismic velocities of 1.3 ms^{-1} can be generated.

The sample assembly is located in the middle of the machine (figure 2b), and consists of 2 solid rock cores sandwiching a gouge layer contained by a Teflon sleeve, and 2 hydraulic grips connecting the cores to the rotary (top) and stationary (bottom) shafts (a more detailed description follows in 'Sample assembly'). Good alignment is crucial for the rotary shear experiments. Beneath the sample assembly a spherical plate is used to adjust the radial orientation of the stationary column. Further misalignments are detected using a dial gauge and is corrected to within 10 µm deviation. In spite of these efforts, some misalignment always exists, and can cause oscillatory signals in the data. Another assembly inside the pressure vessel was aimed to provide the opportunity to do wet experiments under high pressure and temperature, but due to problems this assembly is presently not used.

The sample is axially loaded via the bottom column and normal load is generated using a compex gas cushioning system. In high velocity experiments, sample shortening can be very rapid and the cushioning effect is essential for kee-

ping a more or less constant normal load. In this system, a gas compressor and a gas bottle with a regulator are combined and connected to a bellow cylinder and hydraulic jack, providing a maximum normal load of 8 MPa. When higher pressures are wished for, a gas accumulator can be connected to the system to further boost the normal load up to 40 MPa.

Axial force and torque are measured by two lever-type force gauges attached to the bottom end of the stationary shaft. The rpm of the rotary shaft, and thus the sliding velocity, is measured by a rotary encoder connected to a belt which is in turn connected to the rotary shaft, and a potentiometer. The resolution of the former is too rough for low velocities, so the potentiometer data is used to calibrate the lowest velocity gear, line 1, and to determine the exact moment of velocity steps. The vertical displacement is measured by connecting a to the stationary shaft, which moves upwards as a sample shortens.

2.2 Data logging & processing

Five data signals are recorded on the controller and can be observed real time on the computer; axial force (kN), vertical displacement (mm), torque (Nm), revolution speed (rpm) and potentiometer data (V). The latter two signals come from respectively the rotary encoder and the potentiometer, as described in the previous section.

The current experimental setup, as in all rotary shear experiments involves cylindrical samples, which exhibit a gradient in velocity across their surface. Shimamoto and Tsutumi (1994) define the measured torque as

$$\bar{M}(t) = \frac{2}{3}\pi r^3 \tau(t) \quad (4)$$

And an equivalent velocity v_{eq} (ms^{-1}) such that:

$$dW = v_{eq}\tau S\, dr \quad (5)$$

where dW is the rate of frictional work over the sample surface, τ is the shear stress (Pa), r is the radius of the solid cylinder (m) and S is the surface are of the solid cylinder (m^2). In these formulae it is assumed shear stress is constant over the whole cylindrical surface and only varies with time. However, as the shear strength of materials varies with displacement, and often with sliding velocity, this is never the case due to the existing gradient. This is a very important assumption which may have far-reaching consequences for the absolute values obtained in experimental results. For solid cylinders the equation for v_{eq} (ms^{-1}) reduces to:

$$v_{eq} = \frac{4\pi R r}{3} \quad (6)$$

where R is the rate of revolution (s^{-1}) and r (m) is the diameter of the piston core. From (6) v_{eq} the equivalent displacement d_{eq} (m) is calculated. Recalculating, this means the rate of revolution at r=8.33 mm. V_{eq} and d_{eq} are hereafter termed slip rate (or sliding velocity) and displacement, respectively.

From the measured axial force it is straightforward to calculate the normal stress σ_n. Due to the gas bottle loading system by which normal load is applied, normal stress increases gradually throughout an experiment due to effects from the gas bottle driven loading system. This variation is less than 10% of the total normal stress. To eliminate this trend in the results, we use the coefficient of friction μ ($=\tau/\sigma_n$) to indicate the frictional strength (Coulomb's Law assumed). Steady state frictional strength μ_{ss} is averaged from a manually selected range in the experiment.

Temperature could not be measured during our experiments in the HV2 machine. Since it is important to have an indication about this parameter we assume the slip surface to be extremely thing, so we may employ the following formula for frictional heating (Carlslaw & Jaeger, 1959):

$$\Delta T = \left(\frac{\tau}{\rho c}\right)\sqrt{vd/\pi\alpha_{th}} \quad (7)$$

where ΔT (ºC) is the temperature rise from room temperature, τ the shear stress (Pa), ρ is the density of halite (2160 kg m^{-3}, Mair et al., 2006), c is specific heat of halite (926 J kg^{-1} $ºC^{-1}$, Mair et al., 2006),v (m s^{-1}) is the sliding velocity, d (m) the displacement and α_{th} the thermal diffusivity of halite which according to Kiefer et al. (1976) equals 0.0031 + 9.5 $E^{-4}P$ (cm^2s^{-1}, P in kbars). For a normal pressure of 5 MPa α_{th}=3.15 E-7 m^2s^{-1}. (7) is calculated for dense, pure halite gouge, and it is assumed this is applicable to the mixed gouge as well. Instead of common velocity and displacement, v_{eq} (5) and d_{eq} are used.

2.3 Sample material & Sample assembly

Following Niemeijer & Spiers (2005) analytical grade halite with a grainsize of 90-106 µm and muscovite with a median grainsize of 13µm were used. The muscovite is mined in Aspang, Austria, and provided by Internatio B.V. Both pure halite and mixtures of 80 weight % halite and 20 weight% of muscovite were used as synthetic gouges in the experiments.

In each sample assembly 1 gram of gouge is sandwiched between 2 solid cylinder rock cores with a diameter of 25 mm (figure 2b), resulting in a starting gouge thickness of approximately 1-1.5 mm. The bottom core (S-core) will remain stationary and the top core forms the rotary side (R-

Table 1 *Permeability and relative surface roughness of the rock pistons used in wet experiments. Edited SEM photographs illustrate the relative surface roughenss of gabbro and Berea wall rocks (same scale bar in the middle)*

Rock	Permeability	Relative surface roughness*
Belfast gabbro	Highly impermeable	Low
Au sandstone	~6 * 10^{-17} m^2	Medium
Berea sandstone	~7 * 10^{-14} m^2	High

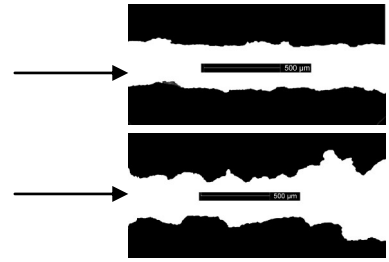

)* all samples are ground with #120 SiC powder. Due to the rock material however surface roughness may differ

core). The surfaces of the piston cores are manually ground with #120 SiC powder to grip the gouge. A 13 mm thick Teflon ring, manually ground to fit tightly around the cores, is slid around the top of the S-core and the gouge is distributed evenly over the surface. Subsequently both cores are put into the machine and are tightened to the stationary and rotary shaft by hydraulic jacks and brought together by applying a normal load.

In high velocity friction experiments, cores of gabbro containing virtually no quartz are generally used. A low amount of quartz is a requirement for these experiments in which high temperatures are reached, because quartz will thermally fracture at around 600ºC (at low normal pressure) due to the transition from alpha to beta quartz and the rock core will break. However, at certain conditions other rock types can also be used. Some of the wet experiments were conducted using permeable sandstone cores (Berea sandstone and Au sandstone), allowing for convenient addition of water (see Experimental procedure). Thermal fracturing is not a problem here, because no wet experiments were done at high velocities. Personal observations suggest surface roughness differs because of the different materials used, eg. the large grainsize of the Berea sandstone. Properties of the gabbro and sandstones are shown in table 1.

2.4 Experimental procedure

Because we aim to reproduce and extend on the halite experiments conducted by Niemeijer & Spiers (2005), the experimental procedure as described by these authors is followed as closely as possible. For the dry experiments this was achievable. However, due to the different machine design the experimental procedure is rather different for the wet experiments.

As the assembly is brought together in the machine, a normal load can be applied. For the dry experiments two different loading approaches were explored to assure gouge layer was well compacted and evenly distributed before the experimental run, namely precompaction (as done by Niemeijer & Spiers (2005)) & presliding. In the first case the gouge layer is compacted at 1 MPa for 10 minutes. In the second case a normal stress of about 0.2-0.3 MPa is applied, and the rotary part of the assembly is rotated back and forth manually, to evenly distribute the gouge until compaction has ceased. A number of comparative experiments for the two loading approached were conducted. Presliding is chosen as the common loading approach for all room-dry experiments.

After preloading/presliding the normal pressure is increased to the desired value, after which the experiment can commence and data is recorded on the computer. When steady state is reached, the experiment is halted. The normal load is removed, and the rock assembly can be taken out of the machine in one part.

The current apparatus setup is not specifically designed for wet experiments, and no pore fluid system, nor any means to measure the pore fluid pressure are present. An attempt to create a pore fluid inlet through the Teflon sleeve failed. The addition of brine is conducted manually, and is different for the gabbro and the sandstone piston cores.

Gabbro is impermeable, and thus brine could not be added through the rock piston. Au sandstone is much more permeable, but still the brine took too long to travel through the wall-rock to the sample and the same addition method as for gabbro is applied. Before both rock cylinders were inserted in the machine and brought together (see 'Sample assembly') ± 0.2 ml of brine is added on top of the gouge. Subsequently the assembly is put into the machine, and the desired normal load is applied instantly (no presliding/ precompaction) and the sample is left to equilibrate for 10 minutes. These 10 minutes include the time it took to load, because normal load had to be set manually and the time to finetune the last percentages of the normal load varies each time. This way possible differences in loading time and thus compaction were eliminated. In the dry experiments this was not done, as compaction did not play so big a role as in these wet experiments. After these 10 minutes the experiment was started.

The Berea sandstone assembly was inserted in the machine and preslided, before addition of the brine. 15 ml of brine is 'injected' with a pipette through the permeable R-core and once the brine has reached the sample (this can be observed in the real time compaction log; as the brine reaches the sample, rapid compaction starts) the desired normal load is applied and as the total loading time is 10 minutes the experiment can be started. During long experiments, the brine is replenished a few times to prevent too much evaporation.

2.5 Microstructure preservation

After a dry experiment, the rock assembly (the two gabbro cores, gouge and Teflon ring) can be taken out of the machine in one part. The Teflon ring is slid down so the gouge layer is just exposed, tape is put around the Teflon ring to create a container around the gouge layer, which is subsequently filled with epoxy.

Preserving the microstructure of wet halite is much more challenging, as crystals will grow rapidly from the brine as experiments are halted, or existing grains may recrystallize. Several techniques were employed to attempt flushing the gouge with hexane to remove the pore fluid, but it proved to be too difficult. In the end the same method as for the dry experiments was applied, i.e. without any flushing but just by sliding the Teflon ring down and add epoxy to the layer.

3. Experimental results

3.1 Dry experiments

The principal aim of this first run of experiments is to try establish a link between the dry experimental results of Niemeijer (2005) on halite-muscovite gouges and the experimental results on the same material conducted in the low-to-high-velocity machine, before commencing with the more challenging wet experiments. Second, shear strength of both pure halite and a mixture of 80% halite & 20% muscovite is explored over a large range of velocities. The effect of a mica on the shear strength can thus be evaluated over an 7 order of magnitude velocity range.

Table 2 gives an overview of the experiments conducted at room-humidity. Two experiments are conducted under a different normal load; these together with two others are used to estimate the Teflon friction (see 'Discussion'). An estimate of the average temperature using during the steady state interval using (3) is included in the table.

3.1.1. Friction coefficient vs. displacement for pure, room-dry halite

Figure 3 shows the friction coefficient and compaction vs. displacement curves for the various experiments on dry halite. Compaction is measured normal to the gouge layer and is taken positive. All of these samples have been preslided at less than 0.3 MPa normal load until compaction has

Table 2 Table of experiments conducted at room-dry conditions, using solid cylinder gabbro pistons

Run #	Composition Ha:Mu	σn (Mpa)	V eq (ms-1)	Loading Presliding	Total d (m)	μ ss	dw (m)	T (°C)
HDR 622	100%:0%	5	1.00E-07	presliding	0.017	0.760	-	15
HDR 616	100%:0%	5	1.0E-06	presliding	0.011	0.746	-	15
HDR 600	100%:0%	5	1.0E-05	presliding	0.024	0.505	0.013	16
HDR 605	100%:0%	5	1.0E-04	presliding	0.124	0.361	0.069	18
HDR 606	100%:0%	5	1.0E-03	presliding	0.426	0.261	0.131	25
HDR 607	100%:0%	5	1.0E-02	presliding	3.200	0.314	0.674	122
HDR 613	100%:0%	5	1.0E-01	presliding	4.840	0.381	0.530	430
HDR 615	100%:0%	5	1.0E-01	presliding	5.940	0.382	0.200	427
HDR 614	100%:0%	5	1	presliding	42.000	0.070	13.700	1042
HDR 316	80%:20%	5	1.00E-06	precompaction	0.040	0.470	0.023	15
HDR 311	80%:20%	5	1.0E-05	presliding	0.050	0.373	0.032	16
HDR 312	80%:20%	5	1.0E-04	precompaction	0.073	0.347	0.032	18
HDR 352	80%:20%	5	1.0E-04	presliding	0.090	0.347	0.027	17
HDR 331	80%:20%	5	1.0E-03	precompaction	0.400	0.313	0.120	31
HDR 334	80%:20%	5	1.0E-03	presliding	0.970	0.293	0.220	34
HDR 603	80%:20%	3	1.0E-03	presliding	0.211	0.340	0.074	16
HDR 604	80%:20%	6.5	1.0E-03	presliding	0.268	0.340	0.120	30
HDR 351	80%:20%	5	1.0E-02	presliding	1.530	0.282	0.100	89
HDR 353	80%:20%	5	1.0E-02	precompaction	1.180	0.284	0.120	70
HDR 354	80%:20%	5	5.0E-02	presliding	0.857	0.359	0.100	149
HDR 355	80%:20%	5	5.0E-02	presliding	2.100	0.357	0.074	250
HDR 323	80%:20%	5	1.0E-01	presliding	0.567	0.501	0.070	338
HDR 324	80%:20%	5	1.0E-01	presliding	1.420	0.472	0.080	320
HDR 330	80%:20%	5	5.0E-01	presliding	22.880	0.110	14.000	872
HDR 329	80%:20%	5	1.0E+00	presliding	20.490	0.050	8.000	673
HDR 608	80%:20%	5	1E-06,1E-07	presliding	-	-	-	15

ceased, and were subsequently loaded to 5 MPa normal load.

All samples show an initial quasi-elastic loading stage followed by a peak in strength, accompanied by rapid compaction. The 2 slowest experiments, HDR622 (0.1 μms^{-1}) and HDR616 (1 μms^{-1}) exhibit some slip weakening after reaching a peak strength of 0.9, but a transition to slip hardening occurs after 0.4-0.5 mm displacement (figure 3a). The slip weakening is accompanied by a small amount of dilatation. Once slip weakening slows and slip hardening takes over, compaction again starts and approaches a steady rate (figure 3b).

Experiments at low velocities (10 μms^{-1} - 1 mms^{-1}) shown in figure 3a-d behave differently; after reaching peak strengths of around 0.7 rapid slip weakening occurs, until a low steady state frictional coefficient is approached. Stick slip occurs in HDR600 (10 μms^{-1}) and HDR605 (100μms^{-1}), initiating directly after peak strength has been overcome. No dilatation occurs in these experiment. The compaction rate is high during the peak strength and initial slip weakening stages and decreases when slip weakening lessens, until a constant rate is approached.

At intermediate velocities (0.01 – 0.1 ms^{-1}) the data again are different (figures 3e and 3f). As opposed to the low strength data, these frictional strength curves are quite irregular. Experiments at these velocities are known to be difficult because samples are usually relatively strong whilst the velocity is quite high (Han, personal communications). The assembly is observed to wobble and these oscillations are reflected in the data. The smaller scale irregularities all have a similar wavelength, corresponding to 1 revolution. Furthermore a resonance effect in the machine may play a role (Togo and Shimamoto, personal communications). Despite the irregularities, data is reproducible and the overall trend can still be analyzed, but one must be aware of gouge loss due to the wobbling. Therefore it is important to watch the compaction data closely. If too big an irregularity occurs there, the experimental data is truncated at that point. After reaching peak strengths of around 0.7, rapid slip weakening occurs until a more or less steady state is reached. The compaction rate is high at the start of the experiment and decreases until a constant rate is reached.

The experiment conducted at 1 ms^{-1} (HDR614) shows an initial peak in strength of around 0.65, followed by rapid slip weakening continuing until a very low steady state strength is reached (figure 3e). Compaction rate is high ini-

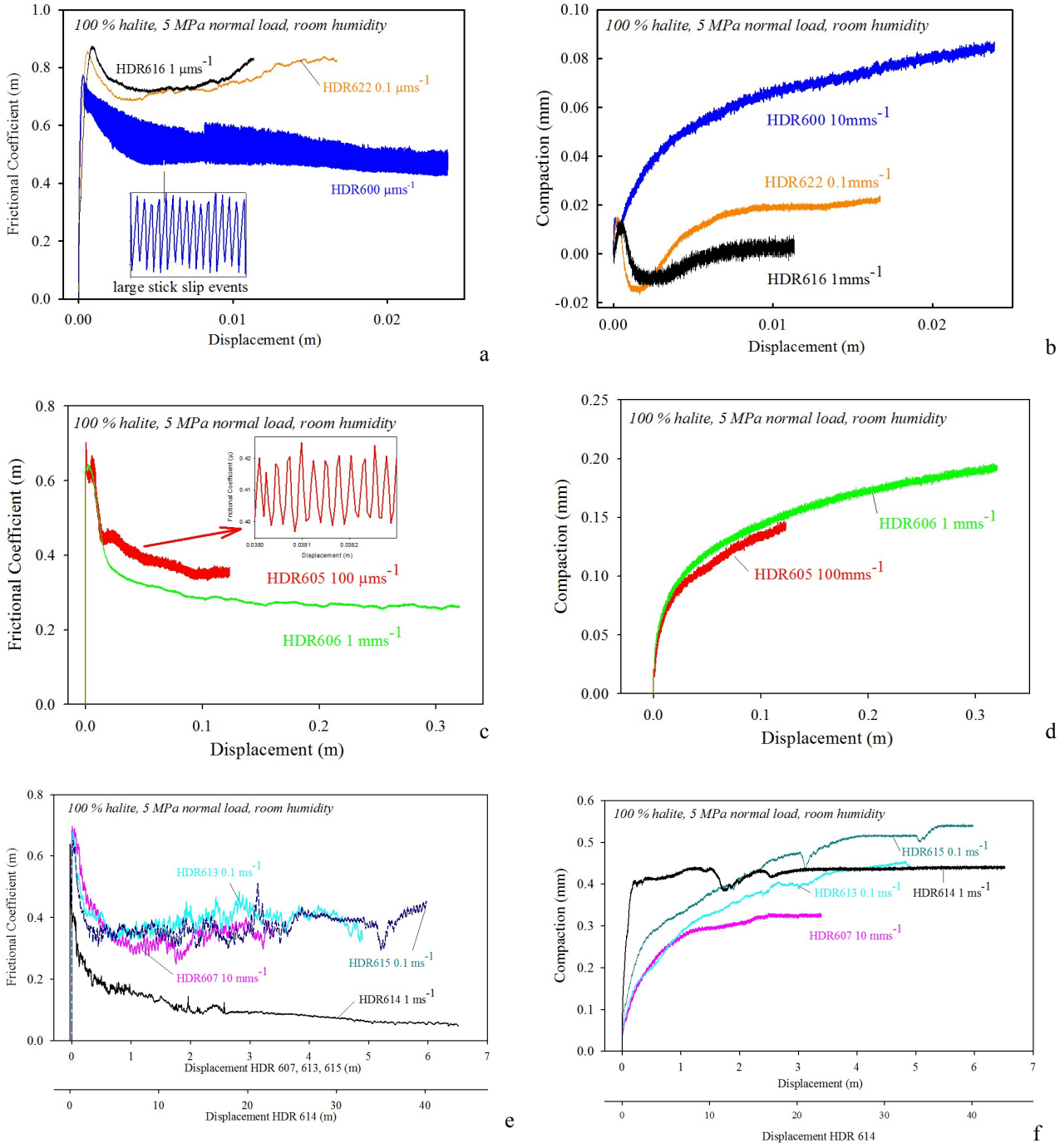

Figure 3 Overview of a series of dry experiments on 1 gram of pure halite gouge at various slip rates using gabbro pistons. A, c, and e show the evolution of the frictional coefficient against the displacement, b, d and f show the vertical displacement (mm) with slip displacement (m).

tially, but as the rate of slip weakening starts to decrease at 1.4 meter displacement, the compaction rate changes abruptly to nearly zero (figure3f). Glassy looking gouge is observed on the surface of samples deformed at this velocity. -

3.1.2. Friction coefficient vs. displacement for room-dry halite + muscovite

The experimental settings are the same as for the pure halite, but instead of a pure halite gouge a mixture of 80% (weight) halite and 20% (weight) muscovite is analyzed. For HDR608 only the first, constant sliding velocity part of the experiment is shown (figures 4a and 4b), as all results shown in this section are of constant sliding velocity.

The slowest experiments (1-100 μms^{-1}) show a sharp peak in strength of about 0.6-0.7, followed by rapid slip weakening until steady state is reached (figure 4a). Stick-slip behaviour is observed in all of the experiments in this velocity range, similar to the experiments on pure halite. HDR608 (1 μms^{-1}) is different from the 1 μms^{-1} experiment on pure halite (HDR616), because it is unstable and shows rapid slip weakening, instead of the slip hardening observed in HDR616.

The experiments from (1-100 mms^{-1}) also experience a sharp peak in strength (0.6-0.7), followed by rapid slip weakening (figure 4 c and e). The frictional strength curve shows an irregular pattern and the data is disturbed by the same oscillatory effects as mentioned in the previous section, as intermediate velocities are reached. The oscillations are even visibly in the compaction curves. Despite the oscillations, reproducibility of the experiments is surprisingly good (eg. compare HDR354 & HDR353) and steady state

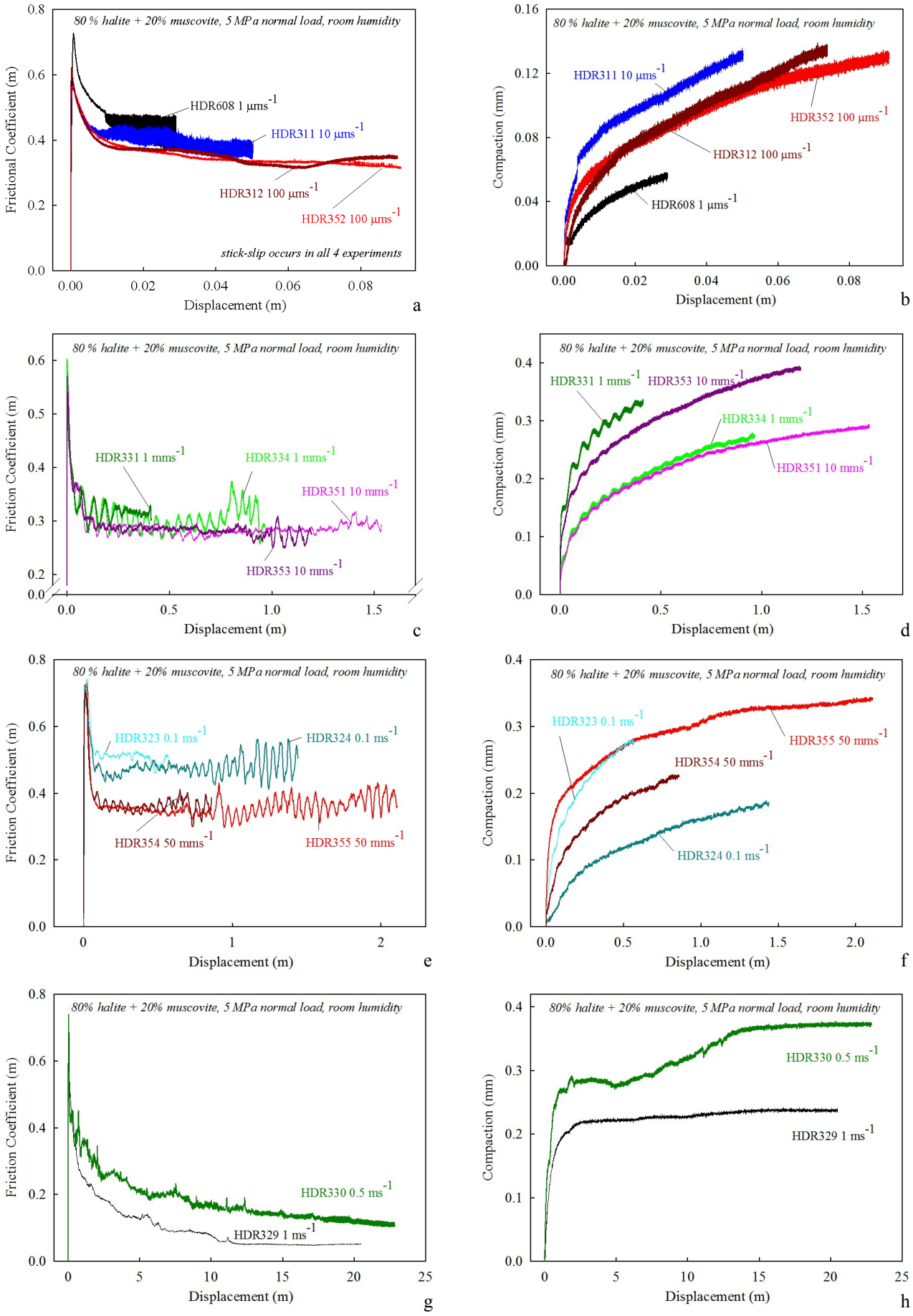

Figure 4

Overview of a series of dry experiments on 0.8 gram halite plus 0.2 muscovite gouge at various slip rates using gabbro pistons. A, c, e and g show the evolution of the frictional coefficient against the displacement, b, d, f and h show the vertical compaction (mm) with displacement (m).

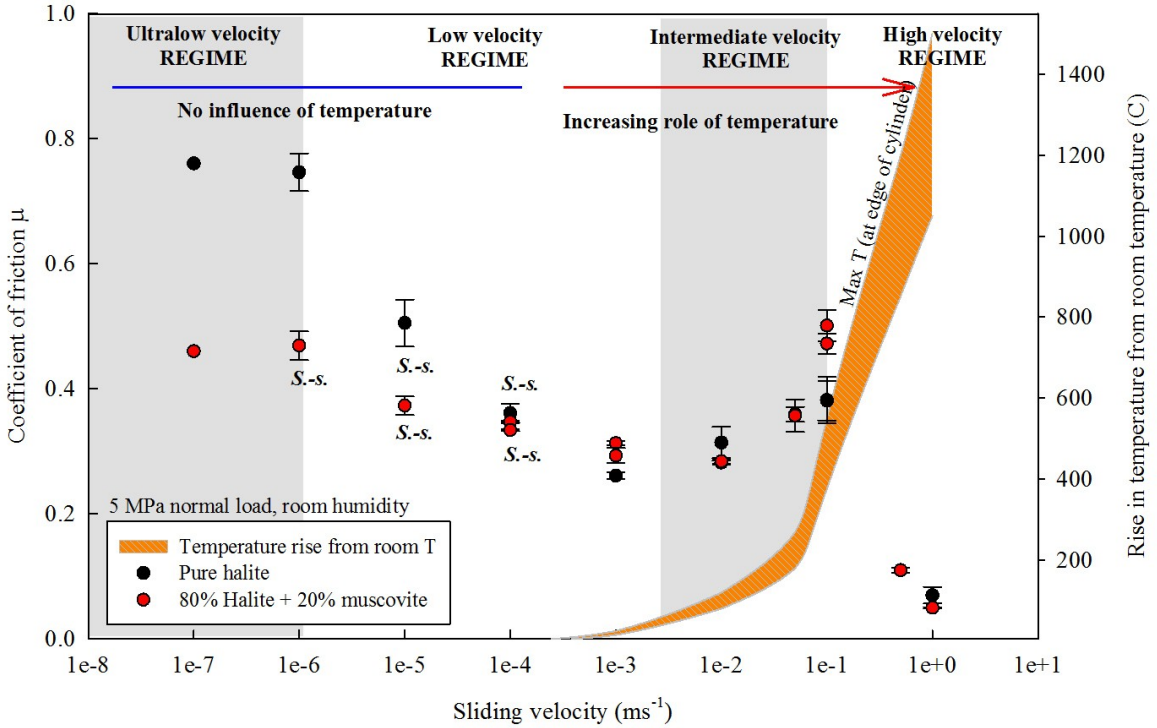

Figure 5 The evolution of the steady state coefficient of friction versus the sliding velocity (ms^{-1}) for pure halite gouge experiments and 80% halite + 20% muscovite gouge experiments at room humidity and a normal load of 5 MPa. An estimate of the average temperature during the steady state interval calculated using Carlslaw and Jaeger's (1976) frictional heating equation is included in the graph (orange area). The upper boundary of this area corresponds to the temperature at the edge of the sample (r=12.5 mm), the lower boundary corresponds to the temperature at r=8.33 mm, at which the v_{eq} is determined.

strengths can be estimated by averaging out the oscillations. The stress drop associated with the slip weakening is different for different velocities and is smallest in HDR323 and HDR 324 (0.1 ms^{-1}). For all experiments up to 100 mms^{-1} compaction is rapid at the start and gradually lessens as slip weakening decreases, until a steady compaction rate is reached (figures 4b, 4d and 4f).

At high velocities (0.5-1 ms^{-1}) peak strength is followed by rapid slip weakening until a very low steady state strength is reached (figure 4g). Compaction is rapid at the start, but shows an abrupt transition to no compaction at all (figure 4h). In HDR330 (0.5 ms^{-1}) only a short period of zero compaction exist, and is followed by a positive compaction rate which flattens out to zero compaction again at larger displacement. Some gouge may have been lost during this experiment.

Three experiments (HDR312, HDR331 and HDR353) have been precompacted before the experimental run, and can be compared with experimental data from experiments that have been preslided and subsequently deformed at the same sliding velocity, HDR352, HDR334 and HDR351 respectively. HDR312 and HDR352 (deformed at 100 μms^{-1}) are practically identical. For the other 2 experiments the frictional strength data is very similar, and also the compaction curves follow the same trend but the absolute amount of compaction is different. This absolute difference may thus be due to the method of loading, and that is why we stick to 1 loading method, namely presliding.

3.1.3. Effect of sliding velocity

A frictional strength vs. sliding velocity plot can now be constructed to demonstrate clearly the effect of sliding velocity. In figure 5 both the steady state frictional strengths of pure halite (black dots) and of the halite-mica mixture (red dots) are plotted. An estimate of the temperature is indicated by the orange area. Temperature only starts to play a role above 1 mms^{-1}.

The main aspect in this graph is the clear rate dependence

Table 3 Overview of the 4 different regimes of deformation for the room-dry experiments and the corresponding frictional behaviour.

Regime	Comp.	Strength with velocity	Dw with velocity	T?	Behaviour with slip distance
Ultralow v	Ha	minor weakening?	-	no	strengthening, stage of dilatation
0.1-1 μm/s	Ha-mu	minor strengthening?	?		weakening, stick slip in 1 μm/s
Low v.	Ha	weakening	increasing	no	weakening, stick slip in slowest
1 μm/s - 1 mm/s	Ha-Mu	"	increasing?		weakening, stick slip in 10-100 μm/s
Intermediate v.	Ha	strengthening from 1 mm/s	decreasing	yes	irregular data (except 1 mm/s)
1-10 mm/s - 0.1 m/s	Ha-Mu	strengthening from 10 mm/s	decreasing		irregular data, oscillations
High v.	Ha	weakening	?	yes	very low μss
> 0.1 m/s	Ha-Mu	"	decreasing ?		

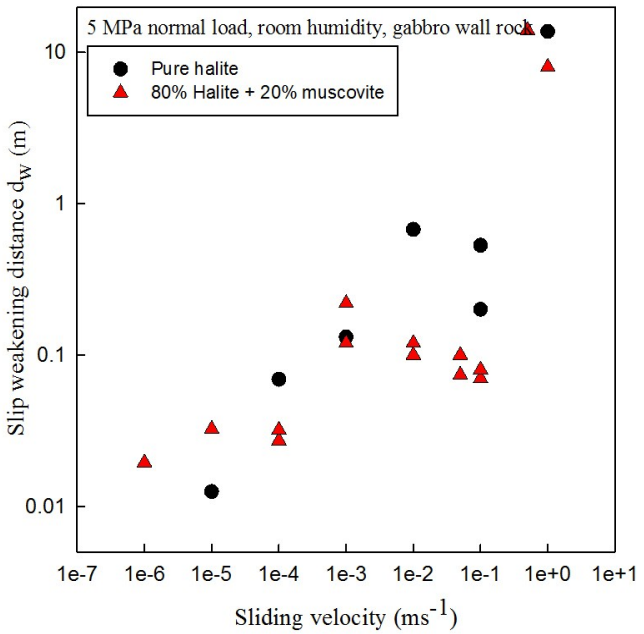

Figure 6 Plot showing the slip weakening distance d_w measured in our data versus the sliding velocity for the pure halite experiments and for the mixed gouge experiments. D_w is the displacement at which 95% of the total drop in strength from peak friction to steady state is achieved.

of the two compositions. Two peaks in strength can be observed in both plots; one peak at ultralow velocities (0.1 – 1 μms^{-1}) and one at intermediate velocities (±0.1 ms^{-1}). What happens at velocities lower than 0.1 μms^{-1} is not clear. No stepping experiments could be conducted to investigate this region, except one (HDR608) where a step from 1 μms^{-1} to 0.1 μms^{-1} is made. However, the instantaneous effect was very hard to see in this experiment, because of the large stick-slip events that are ongoing, second because of the fact that a switch in gear (resulting in a momentary stress drop) needed to be made to achieve this jump and third because the sampling rate is possibly too low to capture the effect.

Figure 5 can be divided into four different regimes, each with their own characteristics; an ultralow velocity regime (0.1-1 μms^{-1}) where not many experiments are conducted and samples may be velocity weakening, equally strong or velocity strengthening depending on the composition, an low velocity regime (1 μms^{-1} up to 1-10 mms^{-1} where there is clear velocity weakening, a intermediate regime (0.01-0.1 ms^{-1}) where samples are velocity strengthening and finally the seismic regime (>0.1 ms^{-1}) where the gouge weakens again. Temperature only plays a role in the two fastest regimes.

Up to 10 μms^{-1} the pure halite gouges are much stronger than the mixed gouge experiments, with a μ_{ss} of 0.72-0.74 versus just 0.5. Also their velocity dependence may differ. However, at low velocities (100 μms^{-1} to 10 mms^{-1}) the steady state strengths of both compositions are similar, both being quite low (± 0.3). Contrastingly, in the intermediate regime, the halite-mica samples are stronger than the pure halite samples. At high velocities both compositions exhibit very low coefficients of friction.

The slip weakening distance d_w, which following Sone and Shimamoto (2009) is defined as the distance required to achieve 95% of the weakening from μ_{peak} to μ_{ss}, is estimated from the dry experiments and plotted in figure 6. The same regimes as described in the previous paragraph may be roughly reflected in this d_w as well. For pure halite, d_w appears to increase with increasing velocity in the velocity weakening, up to the intermediate regime (0.01-0.1 ms^{-1}), where D_w seems to decrease with increasing velocity. In the high velocity regime D_w is much higher, but no trend can be observed as there is only 1 datapoint. For the mixed gouge, d_w increases with sliding velocity from 1 to 10 μms^{-1} but seems to decrease again from 10 to 100 μms^{-1}; more datapoint are necessary in this region. In the intermediate regime (1-100 mms^{-1}), d_w decreases, and in the high velocity regime d_w is much higher.

Table 3 gives an overview of the four different regimes that we recognize and describes the characteristic behaviour belonging to each regime.

3.2 Wet experiments

As described in '2.5 Experimental procedure', gabbro and

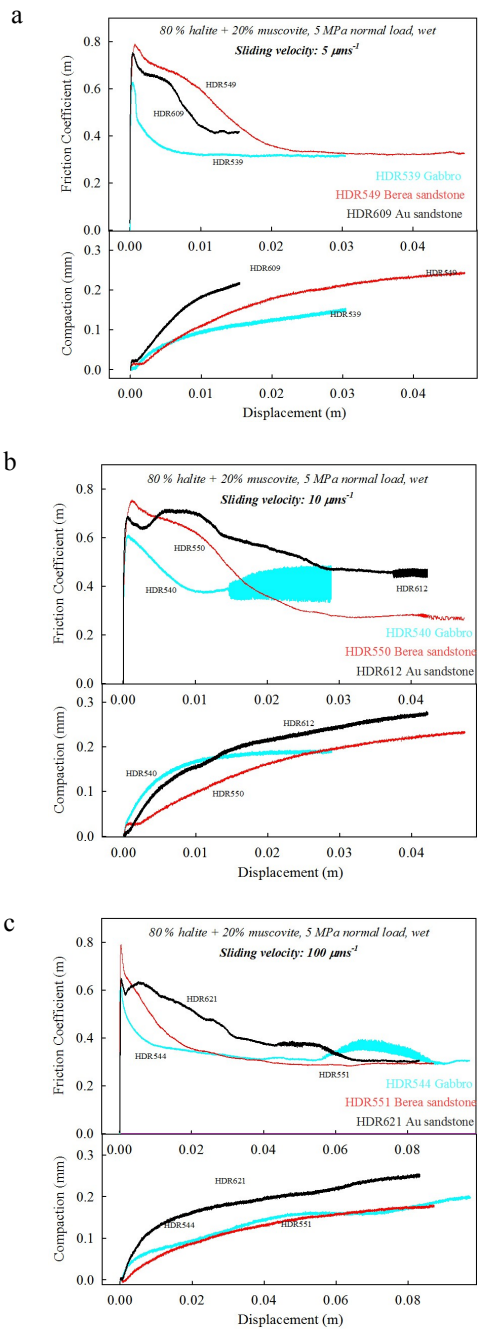

Figure 7 Comparative experiments for three different rock pistons, namely gabbro, Au sandstone and Berea sandstone at a)5 μms^{-1} b)10 μms^{-1} and c) 100 μms^{-1}. All experiments are conducted on 80% halite + 20% muscovite gouges under wet conditions and 5 MPa normal load.

Table 4 List of wet experiments and corresponding experimental conditions.

Run #	V eq m/s	Piston	σn (Mpa)	Total d. m	μpeak	μss	T abs	dw
HDR 609	5.E-06	Au	5	0.0154	0.75	0.416	15	0.011
HDR 612	1.E-05	Au	5	no steady state yet			15	-
HDR 621	1.E-04	Au	5	0.0832	0.65	0.304	17	0.062
HDR 611	2.E-07	Au	5	0.0121	0.72	0.614	15	0.00739
HDR 610	1.E-05	Au	5	no steady state yet			15	-
HDR 581	3.E-08	Berea	5	no steady state yet			15	-
HDR 552	1.E-07	Berea	5	0.0139	0.907	0.565	15	0.0063
HDR 573	1.E-07	Berea	5	0.0217	0.831	0.5	15	0.0104
HDR 561	1.E-06	Berea	5	0.0501	0.88	0.53	15	0.0239
HDR 549	5.E-06	Berea	5	0.0473	0.77	0.326	15	0.0214
HDR 550	1.E-05	Berea	5	0.0474	0.77	0.276	15	0.0246
HDR 551	1.E-04	Berea	5	0.0873	0.79	0.291	17	0.0318
HDR 574	1.E-03	Berea	5	0.265	0.66	0.302	25	0.071
HDR 575	1.E-02	Berea	5	0.5	0.66	0.28	61	0.155
HDR 576	1.E-01	Berea	5	1	0.66	0.294	205	0.311
HDR 539	5.E-06	Gabbro	5	0.0304	0.62	0.317	15	0.00647
HDR 540	1.E-05	Gabbro	5	0.0289	0.61	0.403	16	0.00745
HDR 542	1.E-06	Gabbro	5	0.0429	0.53	0.458	15	0.0154
HDR 544	1.E-04	Gabbro	5	0.0972	0.64	0.326	17	0.021
HDR 582	1.E-08	Gabbro	5	0.00302	0.444	0.35	15	0.00179
HDR 579	1.E-07	Gabbro	5	0.0028	0.65	0.5	15	0.0027
HDR 595	1.E-06	Gabbro	5	0.0931	0.56	0.459	15	0.0048
HDR 543	(5-10-100-1000-100-10) E-6	Gabbro	5	0.32	-	-	-	-
HDR 560	(10-100-5-10-2) E-6	Berea	5	0.22	-	-	-	-
HDR 580	(1-0.1-1-10) E-6	Gabbro	5	0.13	-	-	-	-
HDR 596	(1-0.01) E-6	Au	5	0.045	-	-	-	-
HDR 599	(1-0.03) E-6	Au	5	0.0228	-	-	-	-

sandstone pistons were used for the wet experiments, both with a different method of adding brine and application of the normal stress and each with their own advantages and disadvantages. An overview of all wet experiments is given in Table 4. Nine comparative experiments on the same gouge composition (80% halite + 20% muscovite) at three different velocities investigating the three different assemblies are depicted in figure 7. Different trends can be observed for each assembly.

The gabbro assemblies show the lowest peak in strength, the most rapid slip weakening and reach steady state at the smallest displacements. This is especially the case in the 5 μms^{-1} experiment (HDR539)(figure 7a), but a small note must be made that more brine than in other experiments was added here. Stick-slip is observed in HDR549 and HDR544. Compaction is usually rapid at the start and decreases gradually throughout the experiment. Further observations on other experiments show that reproducibility is not always very well, and some experiments with gabbro pistons show irregular patterns.

The experiments with the Berea sandstone piston do not show a very sharp peak in strength; slip weakening is not so rapid as for the gabbro assembly. Overall the peak in much broader, and a 'hump' in strength follows peak strength. Compaction in the beginning of the experiment is not so rapid, and at all 3 velocities there is even a small stage of dilatation, which is much less (HDR539) or nonexistent (HDR540, HDR544) for the gabbro pistons. It is interesting to note that despite the different frictional strength curve, the steady state strength of gabbro and Berea sandstone pistons reaches exactly the same value in the 5 and 100 μms^{-1} experiments (figure 7a and 7c).

The Au sandstone results are most complicated. In HDR612 and HDR621 the first peak in strength is followed

by a second, broader peak. Curves show some irregularities, and the displacement to reach steady state strength is largest of all assemblies. Compaction is often higher, and like the Berea sandstone experiments a short stage of dilatation is observed near the start of the experiment. The final steady state strength is different from the other assemblies in the 5 and 10 μms^{-1} experiments, although steady state may not have been reached in the first case. It is exactly the same as the μ_{ss} of Berea and gabbro in the 100 μms^{-1} run.

To summarize, overall there is fairly good agreement in the steady state strengths reached for the Berea sandstone and the gabbro pistons, except in the 10 μms^{-1} experiment where the gabbro assembly exhibits very large stick-slip events (figure 7b) . However, before steady state is reached, the strength profiles look different. Apparently the assembly and corresponding experimental procedure influence the results, which is an important and farfetching finding which must always be considered when interpreting the results. When directly comparing experimental data one should compare experiments that have the same assembly. Overall the Berea assembly experiments show the most regular and reproducible data. In the following section only Berea experiments are shown and compared, unless it is deemed fit to include other experiments.

3.2.1. Friction coefficient vs. displacement of wet halite + muscovite

Experiments on halite and muscovite in the presence of brine at constant sliding velocity were conducted from 0.01 μms^{-1} up to 10 mms^{-1}, and the resulting evolution of the

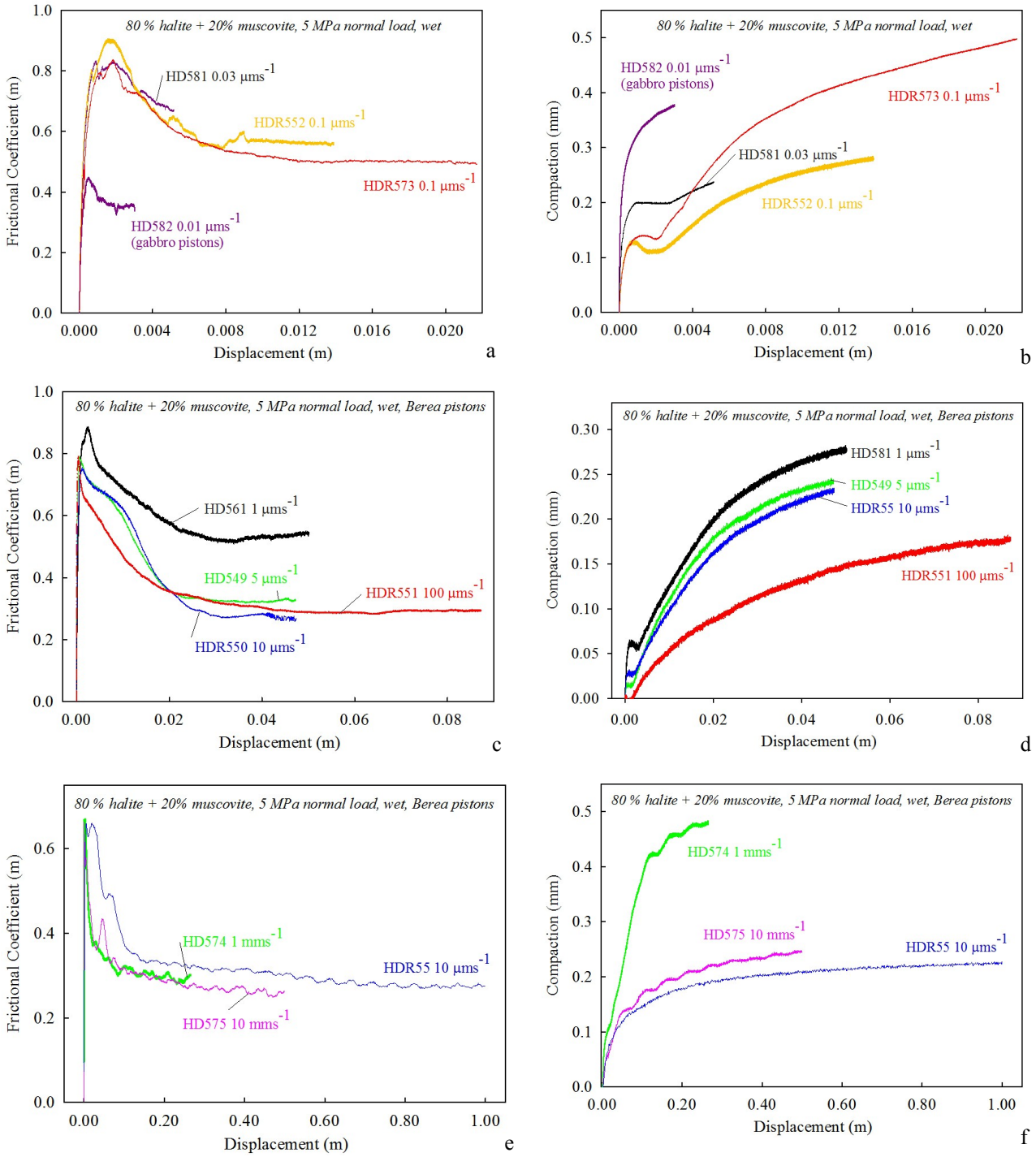

Figure 8 Overview of a series of wet experiments at various slip rates using Berea sandstone pistons. A, c, and e show the evolution of the frictional coefficient against the displacement, b, d and f show the vertical compaction (mm) with displacement (m).

friction coefficient with displacement is shown in figure 8. At 0.1 ms^{-1} steam & salty solution were observed to escape from the assembly, and when taking the sample apart, most of it had dissolved. As this is no longer a realistic analogue system, no experiments at velocities higher than 10 mms^{-1} are analyzed.

As in the dry experiments, samples exhibit an initial stage of quasi elastic loading, accompanied by rapid compaction. Subsequently a peak in the frictional strength is reached, followed by weakening until a steady state is reached.

The slowest experiment, at 0.01 μms^{-1} (HDR582) shows a very low peak strength (μ=0.45) compared to the other experiments (μ=0.7-0.9), and steady strength is also extremely low (figure 8a). Note that this is the only gabbro assembly experiment presented, because no comparative Berea assembly experiment was conducted. Although it is known from the observations in the previous section that gabbro pistons are expected to give a lower peak in strength, these difference are probably too large to be explained by assembly type alone.

The experiments from 0.03 and 0.1 μms^{-1} look pretty similar, although steady state is not yet reached in the former (figure 8a). A transition from initial compaction to a short stage of dilatation is seen in all 3; this transition takes place just before peak strength is reached (figure 8b). When peak strength has been overcome, compaction again commences. The rate of compaction decreases throughout an experiment.. Reproducibility of the 0.1 μms^{-1} experiments is pretty well, except for the absolute amount of compaction. From 1 μms^{-1} up to 100 μms^{-1} similar frictional strength and compaction curves are observed, but overall compaction is much less (figure 8c and 8d).

At the higher velocity experiments (1 – 100 mms^{-1}) rapid slip weakening sets in after peak strength, and no stage of dilatation is observed (figure 8e and 8f). Small machine-related oscillations are again observed in this data, and even show in the compaction curves. Compaction of HDR574 (1 mms^{-1}) is abnormally large.

3.2.2. Effect of sliding velocity

Stepping experiments were conducted to investigate the effect of sliding velocity on the frictional strength. HDR543 and HDR560, 2 experiments conducted in the region 2-1000 μms^{-1}, are depicted in figure 9. Note that the former (figure 9a) is conducted using gabbro pistons, whereas Berea sandstone is used in the latter (figure 9b). More stick-slip is observed in HDR543, which strokes with earlier observations on the influence of the type of rock piston used. The 100 μms^{-1} portions of both experiments show oscillations due to misalignment, average frictional strengths need to be taken.

Both experiments show that upon stepping the velocity up, frictional strength decreases abruptly, although this effect may be somewhat distorted by the large stick-slip events occurring in HDR543. Upon stepping down in velocity, the frictional strength increases again. This effect is clearly visible in for example the step from 1000 μms^{-1} to 100 μms^{-1} in HDR543, where the frictional strength is recovered completely. A remarkable difference between HDR543 and HDR560 is the lack of a peak in strength in the latter upon stepping the velocity down (increase in strength). This may thus be yet another effect of the sample assembly.

More remarkable is that the shape of all of the velocity steps disagrees with the predicted effect from rate and state friction, in which upon stepping up in velocity a peak is

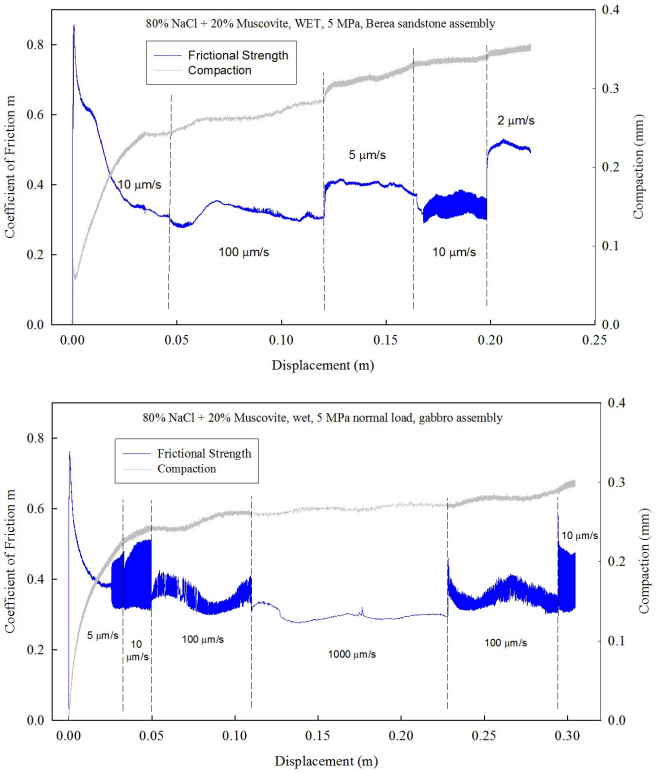

Figure 9 Two comparative stepping experiments in the velocity weakening regime (1-1000 μms^{-1}) at wet conditions using a)Berea sandstone wall-rock and b)gabbro wall-rocks. The coefficient of friction (blue line) and the vertical compaction (grey line) are shown. Note the difference in the onset of stick-slip and the different response to a stepchange in velocity. Both experiments show a response to a change in velocity opposite to what is expected from RSF. Temperature does not play a role in these experiments.

expected, followed by the decay of frictional strength (see figure 1 for typical RSF behaviour in case of an ustep in velocity). In stepping down this effect is the reverse, a downward peak is followed by strengthening. In the presented stepping experiments, the direct effect in stepping down (gabbro assembly) is an upward peak, thus the opposite of the normal rate and state effect. The stepping experiments could thus not be modelled with RSF laws.

Temperature is not expected to play a role in these stepping experiments. The highest temperature reached is during the 1 mms^{-1} stage, where the temperature may increase with 8 degrees above room temperature, or a maximum of 12 degrees rise at the edge of the sample.

In figure 10 data obtained from a number of the wet experiments are combined to give a complete overview of steady state strengths versus the sliding velocity. Experiments were selected based on their reproducibility and overall data quality, and strength values from both constant velocity experiments and velocity stepping experiments are plotted. Error bars denote 1 standard deviation margin. Temperature is plotted in the graph as well (orange area).

Figure 10 again shows a clear slip rate dependence of the sample. A peak in strength appears to exist around 0.1-1 μms^{-1}. At lower velocities the halite-muscovite are velocity strengthening. At velocities above 1 μms^{-1} samples are velocity weakening until a steady state strength of about 0.3 is reached.

The weakening distance d_w is plotted voor Berea and gabbro piston experiments in figure 11. Overall d_w seems to increase with sliding velocity, but from 1 to 10 μms^{-1} it may decrease. Generally the d_w of gabbro wall-rock experiments is lower, as described qualitatively earlier on.

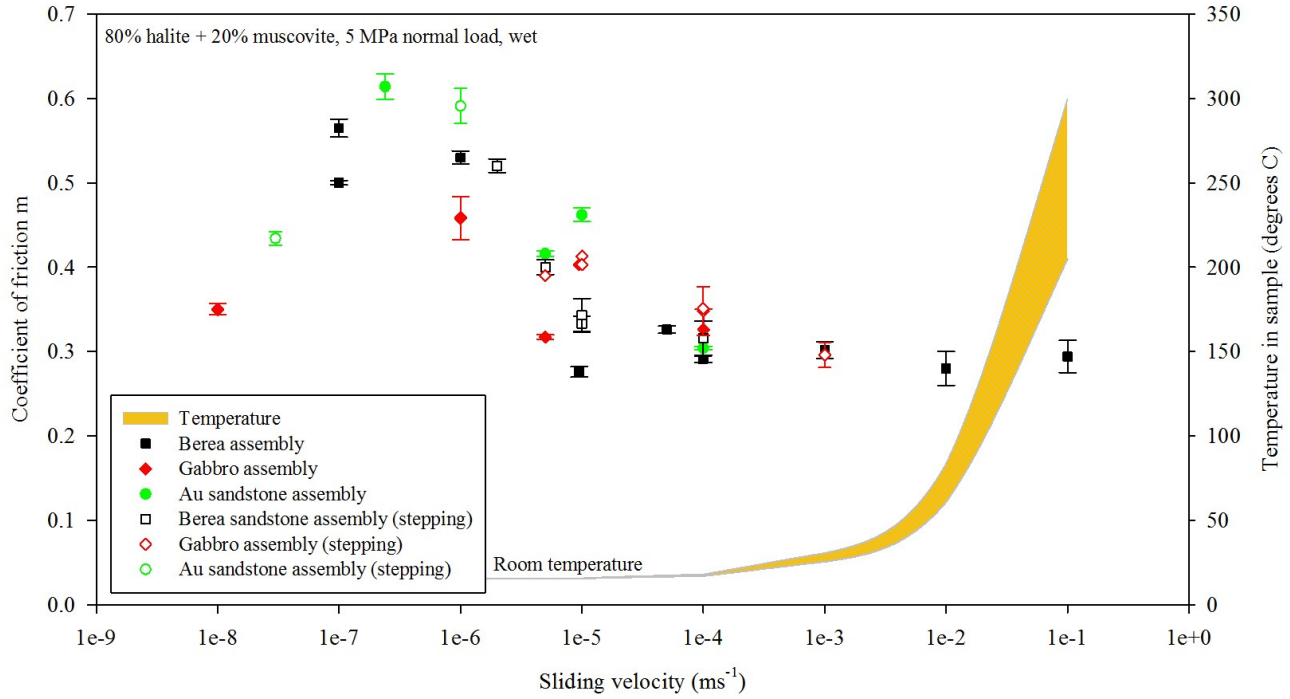

Figure 10 the evolution of the steady state coefficient of friction versus the sliding velocity (ms^{-1}) for 80% halite + 20% muscovite gouge experiments at wet conditions and a normal load of 5 MPa. An estimate of the average temperature during the steady state interval calculated using Carlslaw and Jaeger's (1976) frictional heating equation is included in the graph (orange area). The upper boundary of this area corresponds to the temperature at the edge of the sample (r=12.5 mm), the lower boundary corresponds to the temperature at r=8.33 mm. Results from the three different wall-rocks are shown, as well as data from stepping experiments.

3.3 Velocity jumping

3.3.1. Wet

The wet experiments show a peak in strength around 0.1-1 μms^{-1}. A series of four 'velocity jumping' experiments were conducted to investigate the effect of jumping from the velocity strengthening regime at very low velocities over such a peak in strength simulating a rupture pulse. In one experiment (HDR612) a jump was made from the velocity weakening regime (see table 5 for an overview). Two different assemblies were tested; Au sandstone and gabbro. The Berea sandstone is weakened so much by the presence of brine during the long, slow slip rate experiments preceding the jump that it could not sustain the sudden velocity jump and broke into pieces. In order to jump from velocities in line 1 (< 0.24μms^{-1}) to higher velocities, the gear needs to be switched to line 2 or even line 3. This is done by switching the electromagnetic clutch. However, it was discovered that upon switching the clutch from line 1 to line 2, a moment of free state of the rotary column occurred, resulting in a momentary drop in torque (or shear stress). This effect needs to be taken into account when analyzing the jumps. We assume zero displacement during this moment of free state.

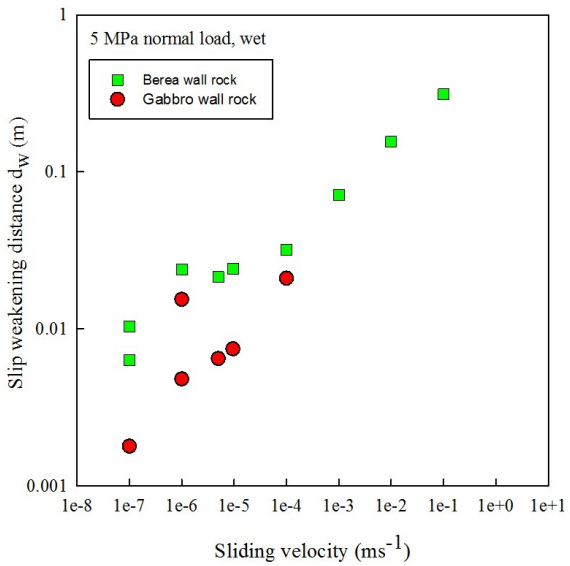

Figure 11 Plot showing the slip weakening distance d_w measured in our data versus the sliding velocity for the the wet experiments. D_w is the displacement at which 95% of the total drop in strength from peak friction to steady state is achieved.

Run #	Old slip rate		New slip rate	Wall-rock	Humidity
HDR 579(2)	1.0E-06	→	5.0E-04	Gabbro	wet
HDR 596(2)	1.0E-07	→	5.5E-04	Au	wet
HDR 599(2)	3.0E-08	→	1.1E-04	Au	wet
HDR 611(2)	2.4E-07	→	1.3E-03	Au	wet
HDR 612(2)	1.0E-05	→	9.2E-03	Au	wet
HDR 597	0.01	→	0.22	Gabbro	room-dry
HDR 598	0.22	→	0.44	Gabbro	room-dry
HDR 617	0.001	→	0.98	Gabbro	room-dry
HDR 618	0.001	→	0.87	Gabbro	room-dry
HDR 619	0.03	→	0.46	Gabbro	room-dry
HDR 620	0.07	→	0.50	Gabbro	room-dry

Table 5 List of velocity 'jumping' experiments conducted in this study. The wet experiments are the second part to a separate constant velocity wet experiment.

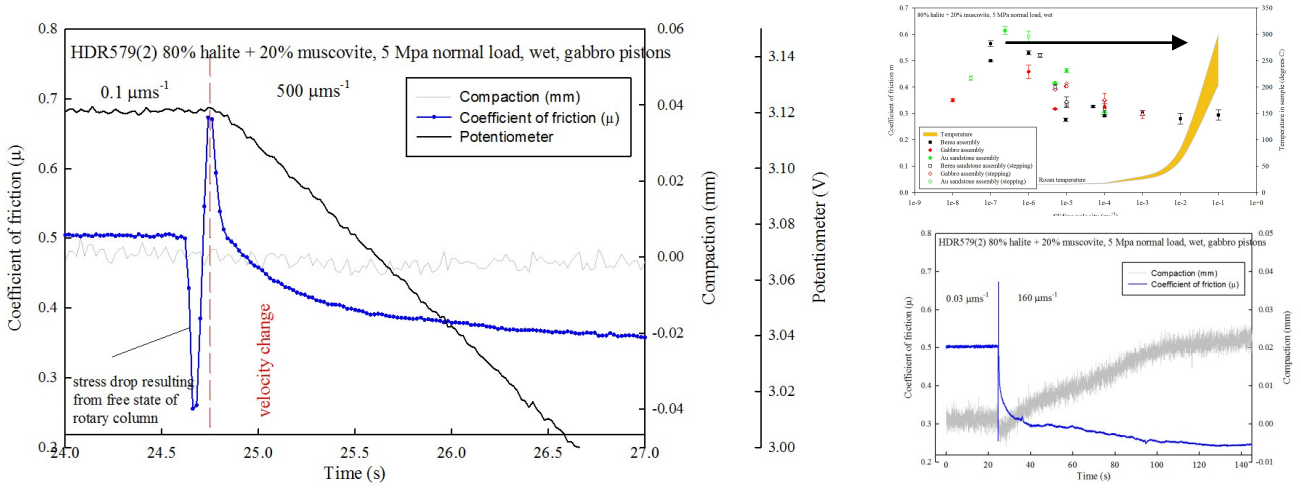

Figure 12 Overview of mechanical data of HDR579, a velocity jump experiment on wet halite plus muscovite, jumping from the strengthening regime (0.1 μms^{-1}) to the weakening regime (500 μms^{-1}). The blue curve indicates the coefficient of friction, the black curce the potentiometer data (V), the grey curve compaction data (mm) a) frictional strength vs sliding velocity plot for the wet experiments indicating the jump in velocity. b) overview of the frictional strength and compaction of the experiment versus time c) zoom of the jump, indicating the frictional strength, compaction and potentiometer data plotted against time. The moment of the velocity change can be determined exactly by the potentiometer data, and is usually very achieved in a very short time.

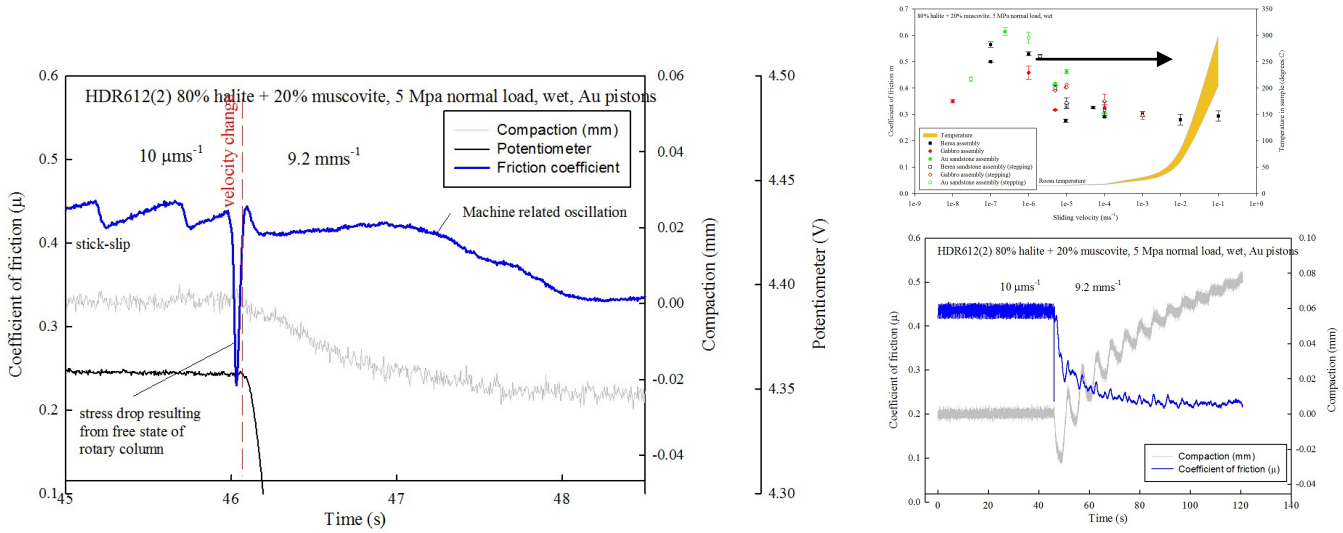

Figure 13 Overview of mechanical data of HDR579, a velocity jump experiment on wet halite plus muscovite, jumping from the velocity weakening regime (10 μms^{-1}) to higher velocity (9200 μms^{-1}). The blue curve indicates the coefficient of friction, the black curce the potentiometer data (V), the grey curve compaction data (mm). a) friction coefficient vs. sliding velocity plot for the wet experiments indicating the jump in velocity of HDR612. b) overview of the frictional strength and compaction of the experiment versus time. Oscillations show clearly in the data. c) zoom of the jump, indicating the frictional strength, compaction and potentiometer data plotted against time. The moment of the velocity change can be determined exactly by the potentiometer data, and is usually very achieved in a very short time. Stick-slip occurs before the velocity is changed.

Run #	**v(0)** µm/s	**v(1)** µm/s	**µ (0)**	**a**	**b1**	**dc1** µm	**b2**	**dc2** µm	**a-b**
HDR579(2)	0.1	497	0.502	0.013056	0.024201	133.641	0.008048	3938.802	-0.019193
			std. dev.	*0.000483*	*0.000474*	*4.172*	*0.000108*	*68.568*	
HDR596(2)	0.1	545	0.658	0.062445	0.086795	79.192	0.017692	9507.428	-0.042043
			std. dev.	*0.000341*	*0.000339*	*0.461*	*0.000034*	*33.154*	
HDR599(2)	0.03	110	0.4435	0.049931	0.053866	194.682	0.020729	25478.578	-0.024664
			std. dev.	*0.00018*	*0.000179*	*0.981*	*0.000024*	*99.877*	
HDR611(2)	0.24	1330	0.573	0.03247	0.047186	161.422	0.017799	9595.057	-0.032516
			std. dev.	*0.000312*	*0.00031*	*1.713*	*0.000058*	*44.303*	

Table 6 Rate and state parameters calculated using Ruina's slip law and 2 state variables. This means the weakening curve is fitted in 2 segments, yielding 2 weakening distances dc and 2 state parameters b1 and b2. Additional linear strain weakening terms of $7.4*10^{-7}$ and $2.4*10^{-7}$ were introduced in HDR579(2) and HDR611(2) respectively. V(0) is the original slip rate and v(1) the new slip rate and µ(0) is the original coefficient of friction.

In figure 12 a jump from the velocity strengthening region is shown (HDR597) and in figure 13 a jump from the weakening regime is shown (HDR612). The jumps are plotted against time instead of displacement; the velocity difference is too large to show clearly the effect with displacement. Potentiometer data (black curves) is used to determine the exact moment of the jump (change in gradient of the potentiometer data). The entire velocity change is usually achieve in less than 0.1 s. The velocity from the moment of the first stress drop (the one due to loss of torque) to the actual visible velocity jump (indicated by the dashed red line) cannot be derived accurately from the potentiometer data, but is probably close to 0 as the rotary column is in a free state.

In figure 12 (HDR579) the stress drop arising from the moment of loss of torque can be clearly observed. This drop is followed by a sharp peak in strength, followed by rapid weakening until a very low steady state is reached. The rest of the jumping experiments from the velocity strengthening regime into the weakening regime show similar behaviour. However, it was found in some of the other experiments conducted with Au sandstone that there is a small delay between the velocity jump and the occurrence of peak strength, whereas this moment is coincidental for the gabbro piston. Thus yet another assembly dependent factor can be added to the list. Despite this small difference, the jumps do show typical rate and state behaviour. However, in HDR612 in which a jump from 10 μms^{-1} (velocity weakening regime) is made to a higher velocity, no peak is observed,. Immediate weakening sets in as the velocity is changed. This is similarly to the velocity steps in the stepping experiments not conform RSF, as in that cast a peak in strength is always expected when stepping up in velocity.

RSF parameters were determined for HDR579, HDR596, HDR599 and HDR611 and are shown in table. All (a-b) values are negative, indicating velocity weakening. No clear correlation seems to exist between the (a-b) value and the magnitude of the jump or the final sliding velocity.

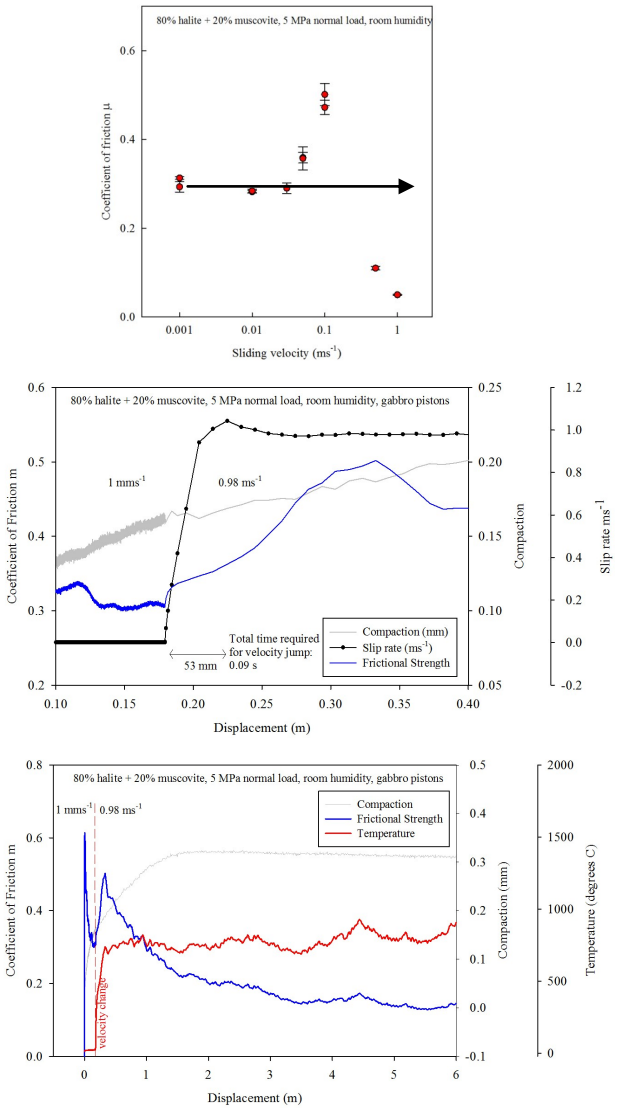

Figure 14 Overview of mechanical data of HDR617, a velocity jump experiment on dry halite plus muscovite, jumping from 1 mms^{-1} to 0.98 ms^{-1}.The velocity is changed by switching the clutch. The blue curve indicates the coefficient of friction, the black curce the potentiometer data (V), the grey curve compaction data (mm) and the red curve the temperature estimate. a) fast end of a friction coefficient vs. sliding velocity plot for the dry experiments indicating the jump in velocity. b) overview of the frictional strength and compaction of the experiment versus displacement c) zoom of the jump, depicting the frictional strength, compaction and potentiometer

3.3.2.Dry

A number of dry experiments were conducted to investigate the effect of jumping over the intermediate peak in strength. The intermediate peak in strength from the dry experiments is covered fully by the line 3 velocity range, so velocity can either be changed by switching the electromagnetic clutch or by pressing numbers. A disadvantage is the noise always present in data around 0.1 ms^{-1}. Experiments conducted at velocities of 0.07 (first part of HDR620) and 0.22 ms^{-1} (first part of HDR598) suffer greatly from this noise, and data is very irregular. Gouge loss is significant. At 0.22 ms^{-1} there seem to be various stages of weakening and restrengthening present. Overall the gouge weakens to a steady state of just 0.13. This is different from 0.07 ms^{-1}, where there might also be stages of weakening and restrengthening, but no overall weakening occurs.

Two of the jumps not suffering (significantly) from the noise are shown in figure 14 (HDR617) and figure 15 (HDR619). As in the wet jumps, potentiometer data is indicated by the black line. Note that the horizontal axis denotes the displacement. In HDR617 a jump is made from 1 mms^{-1} to 0.46 ms^{-1} by changing the gear from line 2 to 3 by switching the electromagnetic clutch. The velocity change is achieved with 0.1 seconds. In HDR619 velocity is covered line 3 and is changed by pressing buttons on the controller twice, taking a little longer (0.25 s).

An overview of HDR597 is shown in figure 16. Because a jump is made to a velocity of 0.22 ms^{-1}, data is very irregular. However, a very broad slip strengthening region is observed before the sample finally weakens. There may be gouge loss during the experiment, as the compaction curve is somewhat irregular.

As an initial velocity of < 0.1ms^{-1} is changed to a velocity >0.1 ms^{-1}, gouges undergoes an initial stage of slip strengthening until after significant displacement a peak in strength is reached. This is observed in all experiments that make a velocity jump over the peak in strength at intermediate velocities. In HDR619 it takes about 0.5 m to until the peak is reached, in HDR617 it takes about 0.15 m. The longest displacement during which strengthening takes place is several meters, occurring in HDR597. The width of the peak appears to depend on the final velocity, the lower this is, the longer it takes before slip weakening sets in. After the peak in strength has been reached, the gouge weakens rapidly to a very low coefficient of friction when the final

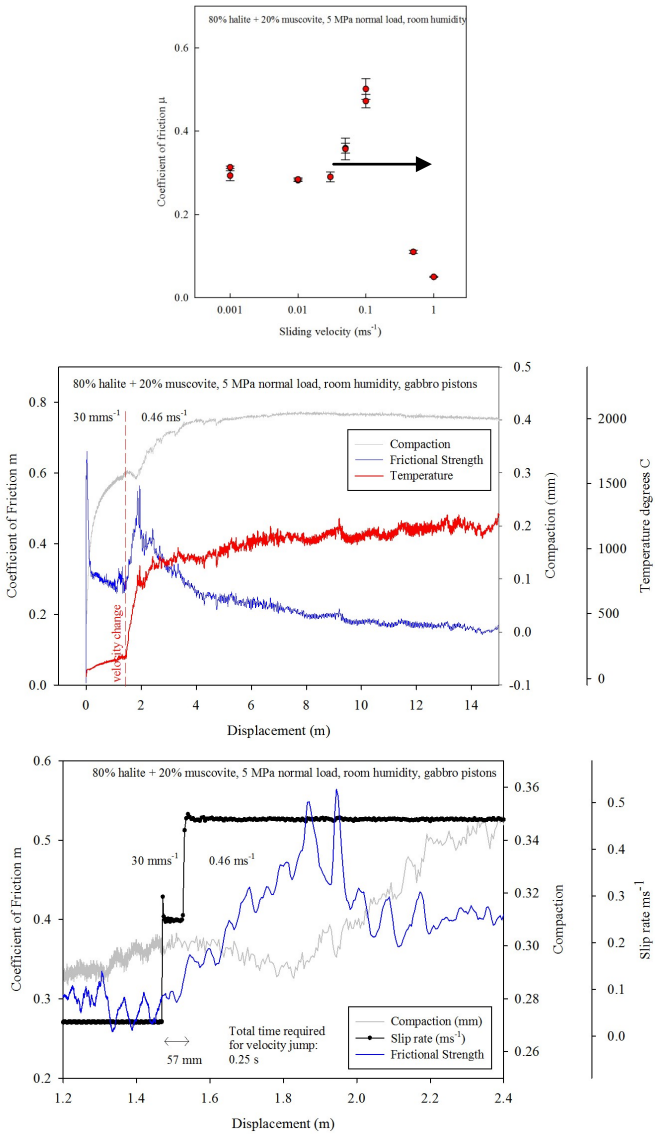

Figure 15 Overview of mechanical data of HDR619, a velocity jump experiment on dry halite plus muscovite, jumping from 30 mms^{-1} to 0.46 ms^{-1}. The velocity is changed by pressing two buttons. The blue curve indicates the coefficient of friction, the black curce the potentiometer data (V), the grey curve compaction data (mm) and the red curve the temperature estimate. a) fast end of the friction coefficient vs. sliding velocity plot for the dry experiments indicating the jump in velocity. b) overview of the frictional strength and compaction of the experiment versus displacement c) zoom of the jump, depicting the frictional strength, compaction and potentiometer data (as an indication for motor speed) plotted against time.

velocity is high (>0.5 ms^{-1})

Reproducibility is quite good. HDR618 is a repetition of HDR617 differing only in that velocity is changed by pressing button instead of changing the clutch, and it shows very similar behaviour.

4. Microstructural observations

Polished sections were viewed in a Scanning Electron Microscope (SEM). The epoxy shows as black in the photographs. There is almost always some detachment visibly, often along the presumed slip surface or along the wall-rock piston, and these gaps are filled with epoxy and show as black structures. Grains may have come apart and are dispersed in the epoxy filling up the extra space. Halite grains shows up as white, and muscovite as grey flakes.

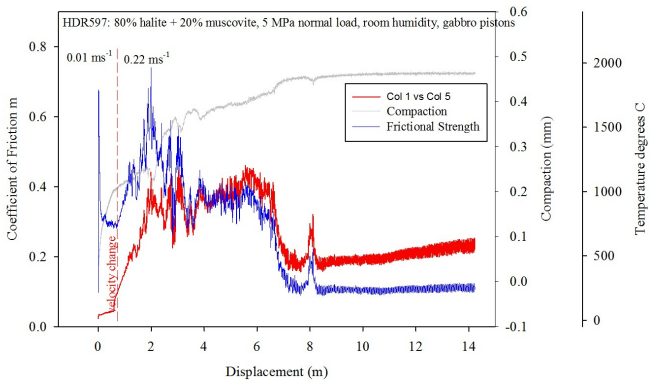

Figure 16 Overview of mechanical data of HDR597, a velocity jump experiment on dry halite plus muscovite, jumping from 30 mms^{-1} to 0.46 ms^{-1}. The velocity is changed by pressing two buttons. The blue curve indicates the coefficient of friction, the grey curve compaction data (mm) and the red curve the temperature estimate.

4.1 Microstructural observations on room-dry pure halite

Four different microstructures, each one developed during an experimental run on dry, pure halite in one of the four sliding velocity regimes recognized in the mechanical data, are presented in figure 17 ; HDR622 (0.1 μms^{-1}, figure 17a, b) , HDR605 (100 μms^{-1}, figure 17c, d), HDR615 (0.1 ms^{-1}, 17e, f) and HDR614 (1 ms^{-1}, figure 17g, h). The gouge structure developed during slowest run (HDR622, final displacement 17 mm) shows numerous halite clasts that appear to be little affected by any deformation, retaining their original grainsize and not showing any sign of being fractured (figure 17a). A relatively wide, boundary parallel zone of smaller, angular grains and larger grains showing signs of cracking is present near the top wall-rock. Presumably during the unloading the sample has broken apart along an irregular surface near the top of this zone, leaving some very fine grained material behind at the gabbro surface. The distribution of fine grained material is laterally heterogeneous. A few of the larger grains are indented in each other.

The microstructure developed during a sliding velocity of 100 μms^{-1} (HDR605) also shows numerous clasts that appear not affected by any deformation. The top part has come apart a little bit, so there is a lot of space between these grains. In contrast to the slower experiment, a very sharp interface, along which the sample has broken up, is present near the bottom gabbro core (B-shear). Fine grained material is present at this interface, especially along the gabbro surface. Larger grains that appear unbroken are present just above the B-shear and are packed very close together, showing indentations.

At 0.1 ms^{-1} no original grains can be recognized. The entire gouge layer consists of angular blocks in a broad range of grain sizes up to more than twice the original size. The big blocks may be aggregates of fine grained material stuck together; when looking on their surface some pores and possibly old grain boundaries are still recognizable. The aggregates are very dense compared to the finer material surrounding them. Near the top and bottom gabbro two B-shears cut through the gouge layer. At the gabbro-halite interface very dense material has accumulated through which no fractures run. Besides these two obvious faults, many faults run through the gouge in Riedel orientation.

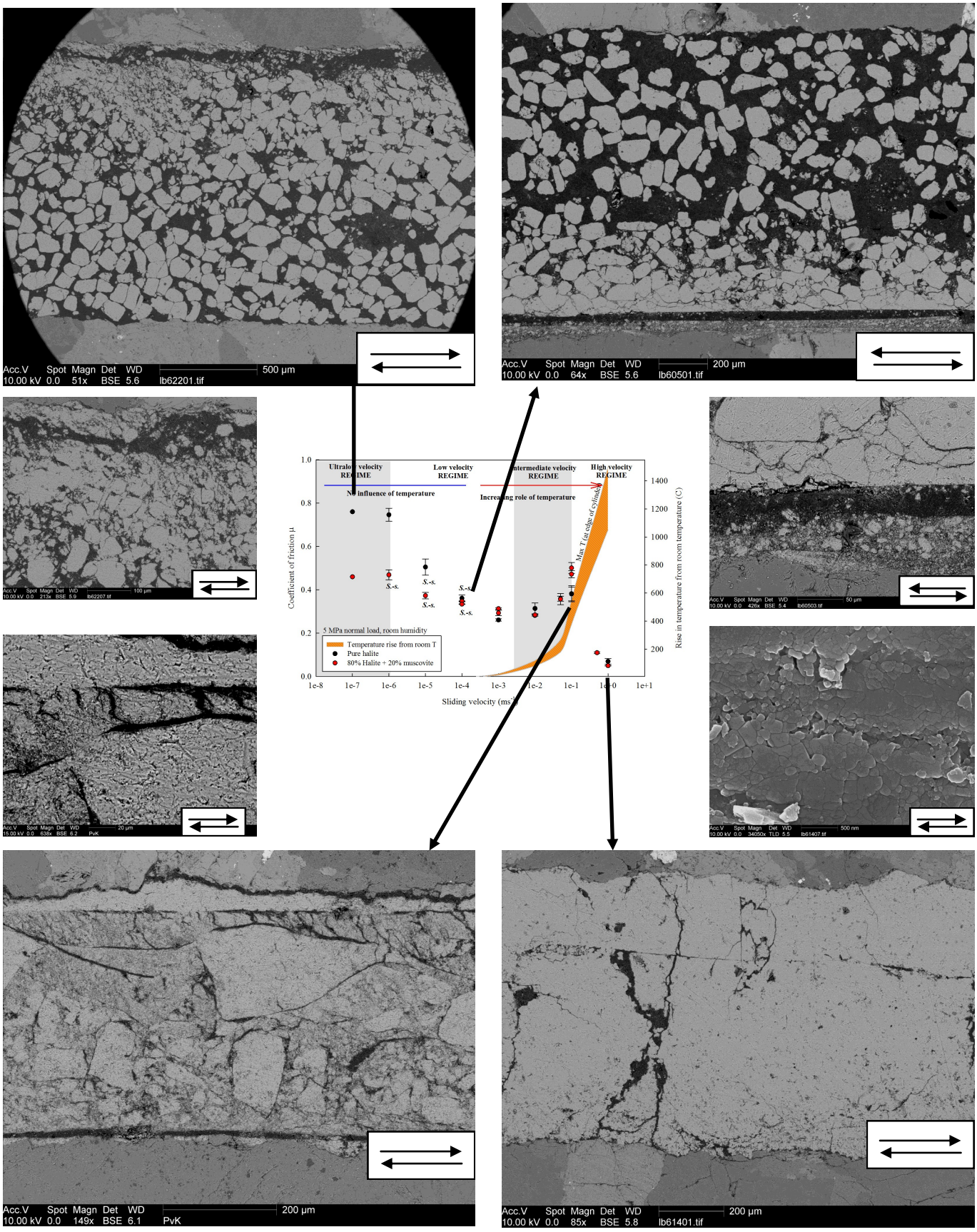

Figure 17 SEM photographs of various microstructures, developed during experiments on room-dry pure halite gouges. The black material is epoxy. The wall rock is gabbro. a)HDR622, 0.1 μms^{-1} b)HDR622, zoomed in on fine-grained zone of c)HDR605, 100 μms^{-1} d)HDR605, zoom in on slip surface e) HDR615, 0.1 ms^{-1} f)HDR615, zoomed view of aggregates g)HDR614, 1 ms^{-1} h)HDR614: zoomed view of planar structure i)Friction coefficient versus sliding velocity plot indicating from which experiments microstructures come from.

The sample deformed at 1 ms^{-1} appears almost completely homogeneous, apart from some secondary fractures in an orientation perpendicular to the wall-rock presumably formed during unloading. There is a planar structure present, just above the middle, which may be a Y-shear going through, but when zooming in the structure is the same as elsewhere in the gouge, except it may be more porous. The material appears very densely packed, not many pores are visible.

4.2 Microstructural observations on room-dry halite + muscovite

Three microstructures developed during mixed gouge experiments, are presented in figure 18 to compare with the pure halite samples.

HDR608 (1μms^{-1}) , shown in figure 18a , came apart during disassembling, and grains are dispersed in a thick layer of epoxy, showing two airbubbles. Above these, the structure has remained quite intact, up to the sharp interface at the top, where the gouge has detached from the top piston. This sharp interface is a B-shear, fine-grained material (possibly a combination of halite and muscovite) has accumulated along it. No material is left on the surface of the top piston. Halite grains in the immediate vicinity of the B-shear show indentations and appear to be dragged in the zone. Further away the halite grains look undeformed, and are separated from other grains by muscovite flakes surrounding them. The muscovite contents seems slightly lower near the B-shear.

The 100 μms^{-1} sample (HDR601) was damaged severely but some fragments still show the through-going Y-shear (figure 18b). Just like its pure halite equivalent, fine grained material has accumulated along this boundary. Furthermore the larger clasts just above the Y-shear are packed fairly close together but are often surrounded completely by muscovite flakes.

The 1 ms^{-1} microstructure looks remarkably different from its pure halite equivalent (figure 18c). A very sharp B-shear is present along the top gabbro boundary. Just below this very localized zone which most likely represents the slip surface, a dense structureless zone of mainly halite is present. Further away from the slip interface halite grains and muscovite seem to be dragged into the slip zone in a ductile manner. Deformation decreases when moving away from the slip zone, and a broad zone above the bottom gabbro grains look unaffected by any deformation.

4.3 Microstructural observations on wet halite + muscovite

Mechanical data from experiments conducted on mixed halite under wet conditions show velocity strengthening at ultralow velocities, forming a peak at 1 μms^{-1}, after which the gouge shows rapid velocity weakening. Two microstructures are investigated and presented in figure 19; one from the velocity strengthening regime (HDR581, 0.03 μms^{-1}) and one from the weakening regime (HDR550, 10 μms^{-1}.

The microstructure developed in the gouge in HDR581 (figure 19a) shows angular and sigmoidal halite clasts of about the original grain size throughout the entire gouge layer, surrounded by muscovite flakes. A Y-shear and Riedel shears cut through the gouge material. At some positions the muscovite is starting to form a foliation wrapping around the halite clasts (figure 19b).

At 10 μms^{-1} the gouge consists out of angular halite clasts surrounded by muscovite flakes (figure 19c). A broad boundary-parallel zone of well-mixed, fine grained halite and muscovite is present below the top sandstone. At the top of this zone, along the sandstone-gouge interface, there appears to be a through-going band of aligned muscovite flakes.

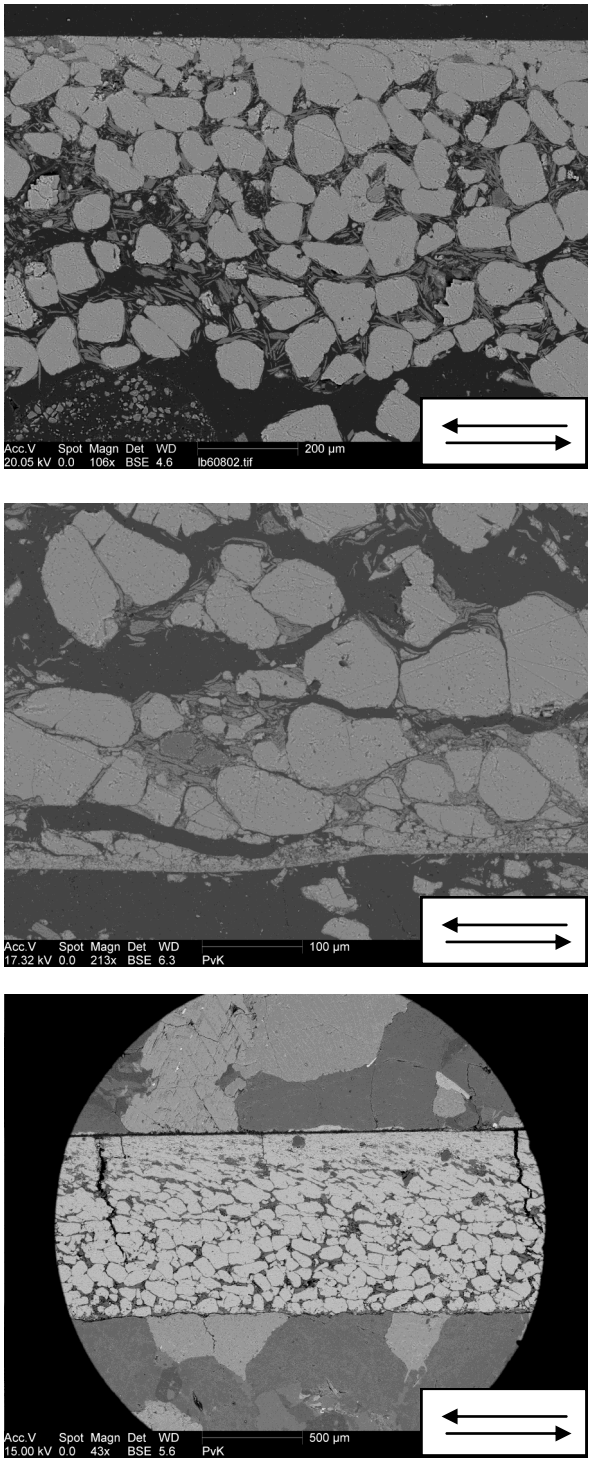

Figure 18 SEM photographs of various microstructures, developed during experiments on room-dry halite plus muscovite gouges. The black material is epoxy. The wall rock is gabbro. a)HDR608, 1 μms^{-1} b)HDR601, 100 μms^{-1} c)HDR329, 1 ms^{-1}

4.4 Microstructural observations on a velocity jump in dry halite + muscovite at high velocities

HDR597 is the microstructure resulting from one of the jumping experiments (figure 20). It was deformed first at a velocity of 0.01 ms^{-1} and a velocity jump to 0.22 ms^{-1} is made. Its microstructure is quite similar to the pure halite microstructure at 0.1 ms^{-1} (HDR615). Large aggregates and

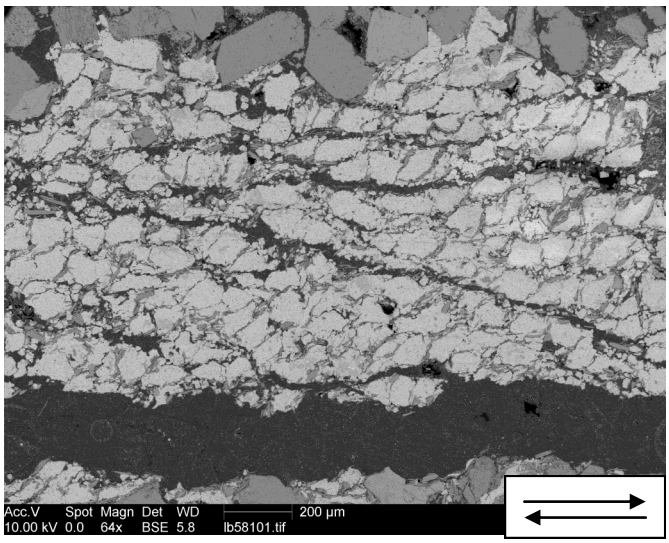

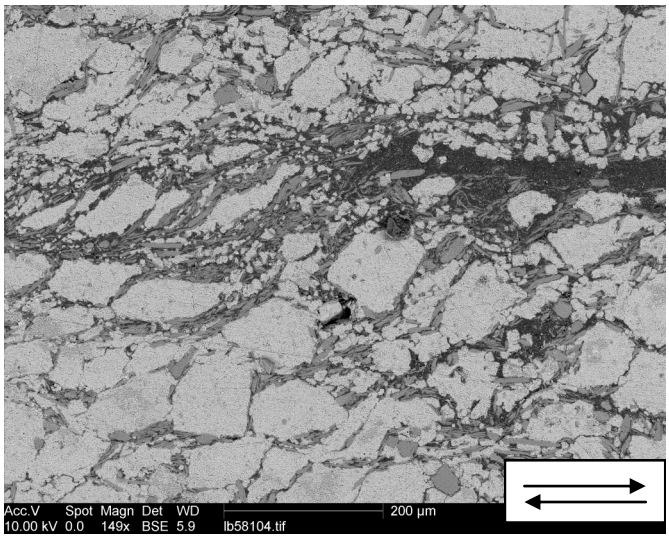

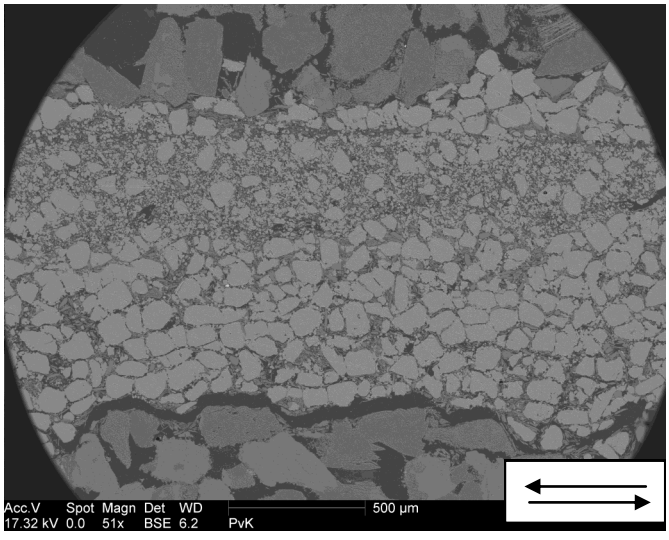

Figure 19 SEM photographs of various microstructures, developed during experiments on wet halite plus muscovite gouges. The black material is epoxy. The wall rock is Berea sandstone. a)HDR581, 0.03 μms^{-1} b) Zoomed view of HDR581 c)HDR550, 10 μms^{-1}

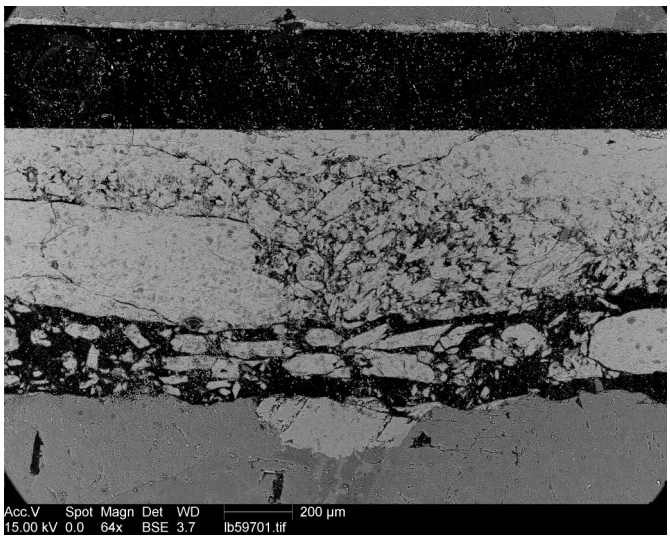

Figure 20 SEM photographs of a microstructure developed during HDR597, a jumping experiment on room-dry halite plus muscovite gouge. A velocity jump was made from 0.01 ms^{-1} to 0.22 ms^{-1}. The black material is epoxy. The wall rock is gabbro. Little white specks apparent all over the section are secondary, possibly resulting from polishing.

many smaller angular fragments (also aggregates) in a wide range of sizes are present, and have been broken up. The density of all the fragments is comparable. A very sharp B-shear has formed near the top piston, the sample has come apart along this interface. The material near this interface is quite dense, unlike the in HDR615 where much finer material with a lot of open space between it had accumulated.

5. Discussion

There are some technical issues of HV2 machine that need to be addressed and/or discussed in order to comment on the reliability of the experimental data and subsequently to try and compare the present data to data obtained by Niemeijer & Spiers (2005). First of all a rotary shear assembly using solid cylinders is used in the HV2 machine, as opposed to the ring used by the aforementioned authors. Constant shear stress over the cylinder area is assumed in the definition of equivalent velocity, but this is not the case. A better definition of the v_{eq} is given by Kitajima et al. (2010). They use a heterogeneous normal load and a heterogeneous friction coefficient (thus a heterogeneous shear stress) over the surface of the cylindrical piston to derive the torque acting on a fault gouge layer, yielding

$$\bar{M}(t) = \frac{2}{3}\pi \int_0^r \mu(r,t)\sigma_n(r,t)r^2 dr \tag{8}$$

We suggest the use of this equation for future research, but could not use it ourselves as it was presented only very recently.

Another problem is that friction between the Teflon ring and the rock cylinders may not be negligible. In order to quantify and check whether we need to correct for this friction three experiments were conducted to estimate it, following the method used by Togo et al. (2009) and Sone and Shimamoto (2009). A plot of peak & steady state normal stress versus shear stress is shown is shown in figure 21. Assuming Coulomb's Law holds at low normal stress, the data can be fit linearly. Furthermore cohesionless gouge is assumed, this would normally let the linear extrapolation go

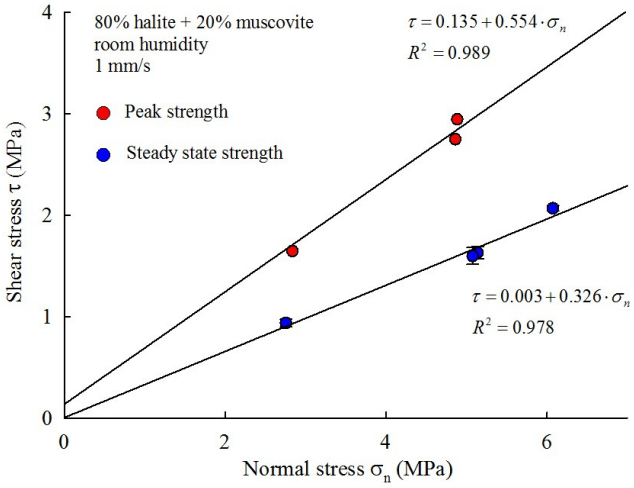

Figure 21 Shear stress against the normal stress for a number of halite + muscovite experiments at 1 mms^{-1}. Assuming Coulomb's Law and cohesionless gouge, the intercept with the y-axis is taken as the Teflon friction. Steady state shear stress was not reached in the 2 MPa experiment and is therefore omitted from this analysis.

through the origin, but this is not the case here. The difference can be interpreted as the Teflon friction, so the interacting with the shear stress axis is thus taken as the value for Teflon friction. Results are shown in table 7.

Values of this study agree reasonably with Togo et al. (2009) and Sone and Shimamoto (2009), but our steady state strength Teflon friction is much lower. Note however that the errors on both Teflon measurements are large, more experiments are required to better quantify the Teflon friction. Based upon the different results for peak and steady state Teflon friction at different velocities, and observations such as that Teflon rings loosen during experiments, Teflon friction is assumed to vary with sliding velocity and displacement. Regarding the difference between Togo et al.'s (2009) finding and Sone and Shimamoto's (2009) findings, which are approximately for the same velocity, it may even be dependent on the manual manufacturing process of the rings.

Shear stress measured in the present experiments vary mostly between 1.5 and 5 Mpa, and Teflon friction usually constitutes (far) less than 10% (0.03 in term of the coefficient of friction) of the measured shear stress. Taking this into account together with its variability and the big error in our attempt to quantify Teflon friction, we have not corrected for Teflon because our experiments span a very broad range in velocity and displacement. It is important however to keep in mind that in reality the coefficient of friction measured may be slightly lower.

Oscillations in the data are observed in many experiments, especially at higher velocities. Despite repeated aligning of the column, misalignment can never completely be eliminated. The wavelength of the oscillations corresponds to one rotation and makes the oscillations easy to recognize. At lower velocities the oscillations are not observed so much, even if displacements are larger than the wavelength. Despite the oscillations, data is still meaningful, because the torque gauge is calibrated under the same conditions (Sone and Shimamoto, 2009).

Another comment must be made on the pore pressure and temperature. In the current setup of the HV2 machine these could not be measured, nor controlled. Especially the pore pressure is an important factor that is missing, and results should be looked at with the possibility of variability in pore pressure and temperature. The addition of pore fluid posed a problem, and 3 different assemblies were investigated to find the best solution. A rough estimate of the temperature was calculated using (3). Observations of melting (0.5-1 ms -1) of halite, taking place at ~800 °C, stroke with the temperature estimate at these velocities, so the estimation seems reliable and may be used to infer processes going on. Temperature starts to play a role from 1 mms-1 onward.

The temperature is calculated at a radius value of 8.33, which is where veq and deq are measured. However, temperatures at the edge of the sample is 1.5 times as high. Lateral heat conduction towards the centre of the circle may cause higher temperatures than those estimated at r=8.33. This is why a broad temperature range is depicted, the upper range of which is the temperature at the edge of the sample, where velocity and displacement are largest.

Now that various technical aspects have been evaluated a better analysis of the data can be made. First of all a correlation between the halite experiment of Niemeijer and Spiers and the HU HV2 experiments is looked at. Subsequently we try to explain the observation made in the dry and wet experiments. Because pure and mixed gouge, low and high velocity regimes (and thus low and high temperature regime), wet gouge and transient behaviour in two different regimes are investigated, the following discussion will span a broad scala of deformation processes and implications for natural fault rock. The aim of the experiments presented in this study was first of all to reproduce or find a correlation between analogue gouge experiments (consisting of halite and muscovite) performed in the ring-shear machine at Utrecht University by Niemeijer and Spiers (2005) in the HV2 machine at Hiroshima University, second explore the behaviour of halite (plus muscovite) over a wider range of velocities to establish a broad strength vs. velocity profile and third to investigate the effect of a sudden jump in velocity over a peak in strength evident from this profile. The final goal is of course to draw conclusion from these analogue results for real fault rocks and earthquakes. Dry experiments performed on pure halite and halite + muscovite gouge show a clear rate dependence; relatively high strengths are found at ~1 µms-1, after which the materials weakens rapidly to very

Table 7 *Teflon friction*

Teflon friction estimate	This study (1 mms^{-1})	Togo et al. (2009) (1.3 ms^{-1})	Sone and Shimamoto (2009) (1.03 ms^{-1})
For peak friction	0.135 ± 0.133 MPa	0.086 MPa	0.179 Mpa
For steady state friction	0.003±0.171 MPa	0.093 MPa	0.105 Mpa

low frictional strength at intermediate velocities, but strengthen again so another peak in strength occurs at intermediate velocities (0.1 ms-1). At high velocities samples melt and frictional strength is extremely low. The presence of muscovite causes lower strengths at ~1 μms-1, does not cause a big difference from 10-1000 μms-1 but yields a higher frictional strength at intermediate velocities as opposed to the pure halite gouge. Wet experiments also show velocity strengthening at ultralow velocities to a peak in strength at 0.1-1 μms-1, followed by strong velocity weakening. High velocities could not be explored for the wet experiments however.

Velocity jumping experiments at low velocities behave conform RSF and show weakening after overcoming a peak in strength. Velocity jumping experiments at high velocities do no behave RSF-wise, but show a stage of inital hardening before a peak in strength is reached and weakening sets in.

5.1 Effect of the sample assembly

Before discussing the possible deformation mechanics operating in the experiments, the influence of the sample assembly on the deformation behaviour needs to be analysed. The comparative wet experiments between gabbro pistons, Au sandstone pistons and Berea sandstone pistons show different results (see table), although the steady state strength is not always so different. One aspect is the onset of unstable behaviour (stick slip), which is best visible in the 10 μms-1 comparative experiments. Stick-slip occurs at the smallest displacement for the gabbro and at much higher displacements for first Au and then Berea sandstone. The slip weakening distance dw is smallest for gabbro, larger for Berea sandstone and largest for Au sandstone. Additional data from the two stepping experiments (Berea vs. gabbro) show different responses to a step change in velocity. Both show behaviour which is opposite to what is expected from rate and state, but the gabbro wall-rock shows sharp transitions, sometimes including a peak, whereas the Berea wall-rock experiment shows more gradual transitions.

The wall-rock have two properties that are different; surface roughness and permeability, plus the addition of brine is different, possibly resulting in a different 'wetness' of the gouge. Differences in the data may thus be related to surface roughness effect or pore fluid effects. Pressurized fluids may dissipate into the permeable wall-rock in the case of the Au or Berea sandstone, because pore fluid pressure cannot be controlled and the wall-rock is permeable, but in case of the impermeable gabbro this is not possible and pore pressure may increase during an experiment, rising above atmospheric pressure. There are multiple ways in which high pore pressures can be generated in the gouge sample. Firstly compaction during shear, for example by ductile creep, may increase pore pressure (Sleep & Blanpied, 1992). Second, experiments conducted on pure muscovite gouges by Zhang et al. (2001) suggest continued shearing of clay gouges may align the micas and create low permeability perpendicular to the alignment, sometimes trapping pore fluids. Another way to generate high pore pressures is by thermal pressurization (Sibson (1973), Wibberley and Shimamoto (2005), Rice (2006)). Finally, dehydration of minerals may also be the cause of high pore fluid pressures (Brantut et al., 2008). The latter two mechanisms however require high temperatures, but temperature does not play a role in the wet experiments up to 10 mms-1, so these can be ruled out instantly as the cause for the different behaviour observed. If dissipation of fluid into the wall rock was the main cause responsible, we would expect the most permeable wall-rock (i.e. Berea sandstone) to be the strongest, or have the longest weakening distance. This is not what is observed, the Au sandstone is usually the one with the longest weakening distance. Gabbro would theoretically be able to build up the largest fluid pressures, but the gabbro wall-rock experiments also show the most unstable behaviour (stick-slip), which cannot be explained by high pore-fluid pressures. Differences in pore-fluid pressures may exist, but they are certainly not the main cause of the different data for different wall-rock.

Surface roughness is the second variable characteristic of the wall-rocks. Experiments at comparable velocities by Niemeijer et al. (2010) on halite using forcing blocks with different surface roughness show an increase in the onset of stick-slip behaviour and the slip weakening distance with increasing surface roughness, which is exactly what is observed in our experiments. Based upon their experimental results and microstructural observations, they interpret the onset of weakening as the transition from Riedel (R) shears to boundary parallel Y-shears and B-shears that localize deformation. Fine grained material is accumulates along the wall-rock gouge interface and eventually forms a through-going boundary (B) shear. This fine material is prone to fluid assisted healing and may cause the unstable behaviour. The rougher the wall-rock interface, the more fine grained material is required to form the boundary shear and the more slip is required for the onset of unstable behaviour. The findings of Niemeijer et al. (2010) seem to fit excellently with our findings. Weakening distance is smallest in the smooth gabbro wall-rock experiments, and stick slip commences at an early stage. In the Au sandstone stick-slip occurs with more displacement, and in the Berea sandstone even later, if it occurs at all. Only the weakening distance of the Au sandstone is larger than expected.

Based upon the similarities between the aforementioned authors and this study, wall-rock surface roughness, and the related localization by formation of boundary shears by accumulating fine grained material resulting in unstable behaviour, is elected as the main cause for the different behaviour of the different wall-rock assemblies. Keeping this in mind, results can be further interpreted.

5.2 Deformation mechanisms in the dry samples

The first series of experiments on both pure halite gouge and mixed gouge was conducted at room-dry conditions. But how dry is room-dry in reality? The gouge is stored in a vacuum container to prevent moisture from adsorbing to it. However, before the experiment the gouge is exposed to room-humidity conditions, which in Hiroshima is 70% in wintertime. Dieterich and Conrad (1984) compared friction experiments on quartzite in an absolutely dry environment with experiments exposed to room humidity, and different frictional behaviour was observed. Dry samples had a higher coefficient of friction, showed less time-dependent healing and lacked stick-slip compared to the room-humid samples. Experiments at room-humidity may yield similar data as their wet equivalents (Morrow et al., 2000). One must thus be careful to name experiments 'dry'. Upon comparing the mixed gouge room-humidity experiments with wet experiments conducted using gabbro cylinders, a very similar coefficient of friction is observed, differing by no more than 0.02. Room-humidity experiments may thus still be influenced by fluid driven processes; pressure solution may also to

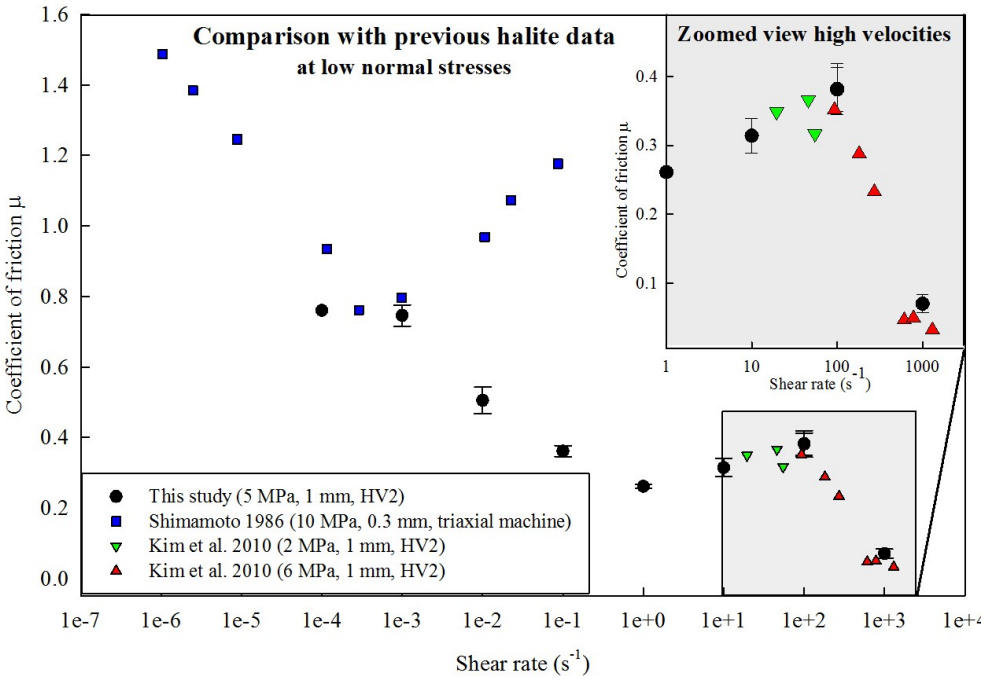

Figure 22 Comparison between steady state friction coefficients of the experiments on room-dry pure halite found in this study with values obtained by Shimamoto (1986) and Kim et al. (2010). Shimamoto (1986) uses a triaxial machine and a gouge thickness of 0.3 mm. Kim et al. (2010) use the HV2 machine and have the same gouge thickness as in this study, namely 1 mm. Steady state strength is plotted against shear strain rate to compensate for the different gouge thickness.

operate here to some extent. Grain indentations characteristic for pressure solution are observed in microstructures in room-dry experiments, implying that it does indeed operate. In some cases the amount of pressure solution going on even seems to be pretty large (eg HDR605, figure 17b). This is important, as it has been shown in many studies that pressure solution processes may greatly enhance (re) strengthening (healing) processes in experimental fault gouges (eg. Niemeijer et al., 2008). Healing can take place by lithification (porosity is decreased, work against the normal stress needs to be done upon reshearing gouge), contact strengthening (grain contacts are strengthened by cementation and mineral precipitation) and compaction which increases the grain contact area (Niemeijer et al., 2008). However, healing rates in 'dry' gouges are estimated to be one order of magnitude lower than in wet gouge (Marone, 1998).

The water present in the dry halite is probably in adsorbed from; no dissolution of the salt nor any visible evaporation take place when higher velocities are reached, while this is the case when a few tenths of a ml. of brine are present in the sample. So mechanical effects from bulk pore-fluids are not expected for the dry experiments, at least not at the lower temperatures.

Dry experiments presented in this study can be divided into four velocity regimes (table 3). Temperature is not of influence in the first two regimes (the ultralow velocity regime and low velocity regime). At 5 MPa and slow slip rates, halite is expected to show brittle behaviour (and thus some solution transfer processes if moisture is present). Plastic behaviour does not occur up to 30 MPa normal load (room temperature) ((Hiraga & Shimamoto, 1987).

5.2.1. Deformation mechanisms for pure halite at room-dry conditions

Pure halite gouges show slip hardening and stable sliding in the ultralow velocity regime (0.1-1 µms-1). An experiment at dry conditions by Niemeijer & Spiers (2005) show exactly the same behaviour for the pure halite at 1 µms-1; stable sliding, a high coefficient of friction and a stage of dilatation at the beginning of the experiment. The microstructure of the 0.1 µms-1 experiment (HDR622, figure 17a) shows a relatively wide zone with a laterally heterogeneous distribution of very fine material and cracked grains. Riedel shears are not observed, but this wide zone points to fairly distributed deformation, which explains the stable behaviour. There is some evidence for pressure solution processes to be operative (grain indentations). The short stage of slip weakening directly after peak strength has been reached may be explained by the grain crushing and fine material accumulating, maybe in a fairly localized zone. Pressure solution is faster in smaller grains, so at some point the fine material may have started healing and thus restrengthening, leading to more distributed deformation and slip strengthening. It might be that gouge will again starts to weaken at higher displacements. In the 100 µms-1 run (HDR605) some stages of slip strengthening are observed before the final weakening to steady state.

At higher velocities (low velocity regime: 10 µms-1 – 0.01 ms-1) , the gouge exhibit slip weakening, unstable behaviour (stick-slip) from early on in the experiment, and velocity weakening up to 1 mms-1. The onset of stick-slip is often linked to the localization of deformation and the accumulation of fine grained material (comminution) prone to healing along the localized zone (Bos & Spiers, 2000, Niemeijer & Spiers, 2005, Hiragana & Shimamoto, 1987, Niemeijer et al., 2010) and this localization plus possibly cataclasisis and grain size reduction are inferred as the slip weakening mechanism at velocities higher than 1µms-1. Besides this unstable behvaiour, localized deformation along Y-shears is related to a lower coefficient of friction and a negative velocity dependence (velocity weakening) (Scruggs & Tullis, 1998), so the localization also explains the velocity weakening behaviour. Both grain size reduction and localized deformation are indeed observed in the microstructures. Fine material accumulates along a very sharp interface. Grains just above this zone show signs of pressure solution to be operating, also more than in the slower experiments. The fine material in the localized zone probably heals and breaks all the time, explaining the observed stick-slip.

Grain size reduction and some pressure solution are also observed in the slower experiments. The difference in behaviour between those and the unstable behaviour at high slip rates may be explained by the relative amount of healing compared to the slip rate.

A comparison with pure halite data from other studies is shown in figure 22. Shimamoto (1986) conducted experiments on pure halite in a triaxial machine at 10 MPa. However, the frictional strength found by Shimamoto (1986) is much higher than in our experiments, and his findings of velocity dependence are opposite, showing velocity weakening up to 1 µms-1 followed by velocity strengthening up to 300 µms-1. Mere speculations can be made to explain the differences. Shimamoto (1986) uses a different normal stress (10 vs. 5 MPa), a different grain size, a different type of halite, a different gouge thickness, and a different apparatus, all of which may give rise to different results. Maybe there is some plasticity going on already at grain contacts, because the normal load is 10 MPa.

At the intermediate and high velocity regimes, temperature starts to play a big role, and processes distinct from those at low velocities are expected. Velocity strengthening and a decreasing dw are observed in the intermediate region. Experiments are difficult and data is noisy, but they are reproducible and clearly show a peak in the frictional strength vs. velocity profile at 0.1 ms-1. This is not observed by Kim et al. (2010), who conducted experiments in exactly the same experimental setting on pure, room-dry halite in the range of 0.02-1 ms-1 at low normal stresses (see also figure 22 for comparison) They conducted a few experiments at intermediate (termed subseismic in their study) velocities, but although they found similar friction coefficients, they did not recognize velocity strengthening. Too little data is shown in their paper, but velocity strengthening could just as well be operating based on the presented information. They use cooking salt of a different grainsize, as in Shimamoto's (1986) experiments, so maybe that is the cause for the difference.

Microstructural observations from this study show large angular block that are probably dense granular aggregates together with a lot of smaller, fractured material. Y-shears and Riedel-shears cut through the entire structure. Material at the boundaries and in the aggregates appears denser than the small grained stuff. Most likely the halite was deformed and grainsize was reduced and the small grains were 'welded' together forming a denser structure which was quite strong. This healing may have taken place by pressure solution for example, which becomes faster with decreasing grainsize. At the intermediate velocities grains may become so small due to cataclasis, that healing becomes very fast, and thus strengthening the material rapidly. This strengthening may then have led to breaking up of the dense mass by more distributed deformation, yielding the aggregates and finer material. So most likely the mechanism by which the halite is deforming at the steady state is an interplay of the formation of strong material by healing, and distributed fracturing of this material. Kim et al. (2010) find quite similar microstructures and conclude cataclastic flow is still going on at these velocities.

Friction coefficients and dw's obtained by Kim et al. (in press) at velocities above 0.1 ms-1 (strong velocity weakening to a friction coefficient of 0.05 at 1 ms-1) match extremely well with results presented in this paper (figure 22). However microstructures are different. We find a very dense, homogenous polycrystalline mass of halite, with little structures in it. There may be a principal slip surface, but no different microstructure is observed near this planar feature. Kim et al. (2010) find a localized slip layer consisting of very fine equiaxed grains which they interpreted as melt. This slip layer is bounded by a slow slip-rate zone composed of polycrystalline halite ribbons elongated obliquely to the shear zone boundary. The latter are similar to semiplastic halite structures found by Shimamoto (1989). Kim et al. (2010) interpret deformation of halite in the high velocity regime to occur by frictional melting (T<800 ºC) , which heats the surrounding rock to temperatures high enough (average 690 ºC) to induce plastic deformation. We cannot produce hard evidence that melting has occurred in our experiments, but as we measure a similar low shear strength as measured in Kim et al. (2010)'s observations, there may have been some melt. Maybe our slip surface was so thin we could not find it back, and the rest of what we see may have deformed plastically. To confirm additional research needs to done to see whether an LPO is present.

5.2.2. Deformation mechanisms of halite + muscovite at room-dry conditions

The muscovite containing gouges all show slip weakening, sometimes stick-slip behaviour and velocity weakening from 1 µms-1 up to 0.01 ms-1. This means in the ultra-low velocity regime (0.1-1 µms-1) the behaviour with slip displacement is different from that of pure halite, as pure halite samples show a short stage of slip weakening, but then slip strengthening starts to occur. The pure halite compaction curves also show a short stage of dilatation, which is not observed in any of the muscovite containing samples. The microstructure at 1 µms-1 shows of the mixed gouge shows a very sharp localized slip surface near one of the pistons, along which fine material has accumulated. Near this slip surface muscovite seems to be present in lesser concentrations than in the undeformed part of the gouge. Evidence for pressure solution is present in the halite grains near this B-shear. Apparently the degree of localization is the main factor causing the different behaviour with slip. Phyllosilicates in between halite grains may inhibit contact healing (Bos & Spiers, 2000). There may initially be less healing and thus less restrengthening, so deformation may not become very distributed. In the localized zone where fine material accumulates healing is probably going on, causing the observed stick-slip behaviour. Also the steady state strength of mixed gouge is lower than its pure halite equivalent at the slowest velocities (0.1, 1 and 10 µms-1). The addition of a weaker material is known to weaken frictional strength (Kawamoto & Shimamoto, 1998), and this forms an argument for the lower strength of the mixed gouge.

Localization again seems to be the controlling mechanism of deformation in the low velocity regime, up to 0.01 ms-1. Microstructural observations developed during a slip rate of 100 µms-1 (HDR601) support this, showing a very localized B-shear along which fine grained material has accumulated. They are very similar to the 1 µms-1 microstructure (HDR601). Pressure solution evidence is present in this sample as well, but not as much as in the pure halite equivalent, probably due to the presence of muscovite which inhibits contact healing by pressure solution. Lesser pressure solution and thus lesser healing by this process may explain why the amplitude of stick-slip at this velocity is smaller than the amplitude of the pure halite sample at the same velocity.

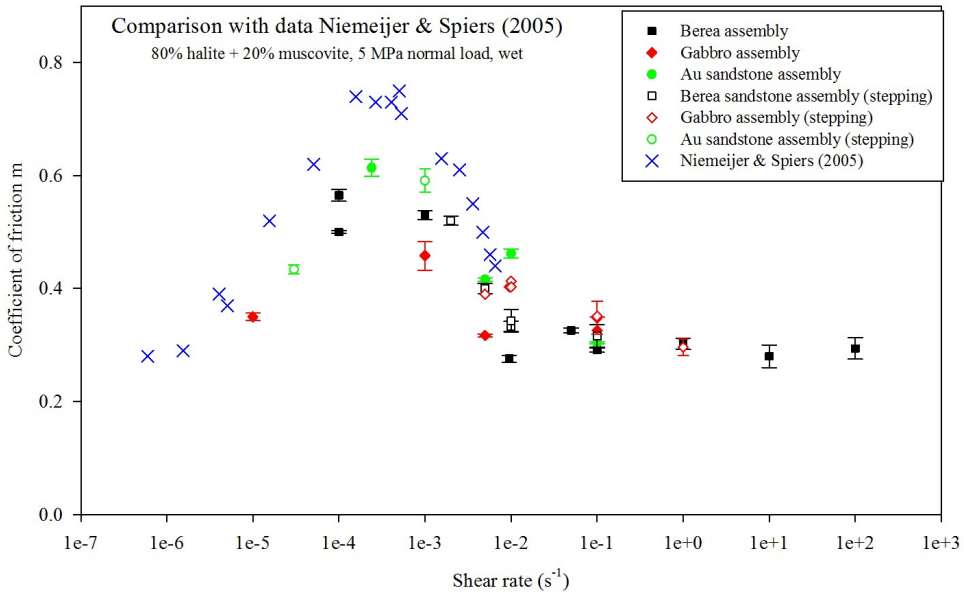

Figure 23 Comparison between steady state friction coefficients of the wet experiments found in this study compared to those presented by Niemeijer & Spiers (2005). The starting gouge thickness is different, 1 mm in this study versus 2 mm in Niemeijer & Spiers (2005) and therefore the coefficient of friction is plotted against the shear strain rate. .

In the intermediate regime the mixed gouge strengthens again just like the pure halite gouges. They become even stronger than the latter, reaching a coefficient of friction of about 0.5 We can only hypothesize on why muscovite apparently makes the gouges slightly stronger. Muscovite may dehydrate at 400 °C (Mariani et a., 2006), a temperature that based on our calculations may well be reached in this regime. Maybe water may have an effect on the deformation process going on here. If the aggregates indeed form by a healing process which is dependent on water such as pressure solution, this will be enhanced by the water released from the dehydration reaction, thus increasing the restrengthening rate.

Frictional strength is very similar to pure halite data in the high velocity regime. The microstructure at 1 ms-1 however is very different. Instead of a fairly homogeneous mass a very hetereogeneous structure is observed with intensity of deformation increasing towards a very localized slip surface. Displacement is 20 meters as opposed to 40 meters for the pure halite sample. Apparently the presence of muscovite again favours localization. Cubic grains found at the slip surface may form some indication for melting.

5.3 Deformation mechanisms in wet halite + muscovite gouges

The wet experimental data is very similar to the experiments by Niemeijer & Spiers (2005), as can be seen in a comparative plot of the coefficient of friction versus the shear rate (figure 23).

Velocity strengthening is found at ultralow velocities (<1 µms-1) and velocity weakening occurs at velocities larger than that. Our mechanical data is different from the Utrecht experiments in that during a constant velocity experiment we find a peak followed by slip weakening, whereas in the Utrecht experiments no slip weakening is observed. The amount of slip weakening is least in HDR582, the slowest experiment. However, the observed microstructure at 0.03 µms-1 show sigmoidal clasts with muscovite around them, indicating the formation of a muscovite foliation, very similar to Niemeijer & Spiers (2005)'s microstructures. Definitely the same process is going on. Following Niemeijer & Spiers (2005,2006,2007) this means frictional-viscous mechanism (slip of halite grains on a muscovite foliation accommodated by pressure solution) is presumed to be operating at the lowest slip rates (0.01- 1 µms-1).

For velocities above 1 µms-1 the microstructure show a zone with fine-grained material. Muscovite and halite are very well mixed in that zone, indicating granular flow in the material. We infer cataclasis and granular flow to be operating, like in the experiments of Niemeijer & Spiers (2005). The slip weakening and velocity weakening can again be explained by the previously described localization process, as stick slip is observed in some of the experiments. As also mentioned earlier, the onset of localization depends on the surface roughness of the wall-rock type, it is observed much more in the gabbro wall-rock experiments. We only observed a wet experiment deformed by Berea pistons (the roughest). The slip zone is still fairly broad but might localize more and more, as would be expected from our analysis of surface roughness effects. Presumably the zone of deformation would be much thinner if the same experiment was conducted using a gabbro wall-rock.

Niemeijer & Spiers (2006) propose the velocity weakening in the same gouge material to occur by granular flow plus a competition between intergranular sliding and pressure solution controlled compaction. As porosity increases, the inclination of the sliding grain contacts is reduced, and intergranular friction decreases, resulting in the weakening. No localization is observed in their microstructures. However, we favour localization as a main weakening mechanism in our gouges, because we observe a more localized zone of deformation in the microstructures, because of evidence on the effect of localization from more recent experiments by Niemeijer et al. (2010) and because it explains the wall-rock dependent behaviour very well. A combination of both mechanisms may occur. Maybe shear displacements in Niemeijer & Spiers (2006) were not large enough to form boundary shears. Their wall-rock appears relatively rough, so localization will probably take a long time. In the Berea wall-rock experiments (high surface roughness), unstable behaviour (and thus localization) occurs only after large strains, but it is definitely happening eventually, as can be observed in the stepping experiment HDR560.

The stepping experiments do indicate that most of the behaviour is reversible upon stepping down in velocity; approximately the same steady state frictional strength is recovered at the same velocities.

The direct effect of the stepping experiments is hard to explain. It does not correspond to the typical behaviour expected from rate-and-state-friction, and if anything, it is even opposite to that. Steady state strengths are similar to those obtained in constant velocity experiments, so the stepping experiments are not meaningless. Temperature is not expected to be of any influence, as the highest temperature estimated is 25-30 °C (during the 1 mms-1 stage). HDR543 and HDR560 are both conducted in line 2 by pressing buttons. It is strange that typical RSF behaviour is observed in HDR580 and all 4 jumping experiments conducted from line1, almost suggesting it may be related to the apparatus. However, when analyzing potentiometer data, the change in velocity is equally swift in both. It is also not related to the type of assembly, as both Berea and gabbro show the same direct effect.

5.4Jumping over a peak observed in the frictional strength versus sliding velocity data

Jumps in velocity (basically large velocity steps, often of three orders of magnitude) were conducted in mixed halite-muscovite at 1) wet conditions and slow slip rates and 2) room-dry conditions and high slip rates. The aim of the first set of experiments is to investigate the effect of an earthquake rupture (simulated by the velocity jump) coming in on a creeping (stably sliding) fault (the velocity strengthening regime as found in our wet data at velocities lower than 1 µms-1). In other words, a jump over the peak in frictional strength at low velocities (see figure 10) is made. The aim of the second set of experiments is also to gain insight into the transient portion during earthquake rupture and especially into the effect of the velocity strengthening portion just before great weakening occurs at high velocities which may approach seismic velocities as in nature. Such a velocity strengthening portion may act as a barrier to earthquake propagation. Several jumps are made from the intermediate velocity regime (which is also velocity strengthening) into the high velocity regime, in room-dry gouges as wet gouge could not be deformed at such large sliding velocities.

5.4.1Velocity jumps in wet halite plus muscovite gouges at low sliding velocities

The low velocity jumps at wet conditions from low velocities into the weakening regime show a sharp peak in strength against displacement (see figure 12), followed by an exponential decay in frictional strength, which could be modelled with Ruina's RSF equation, using two state functions and in some cases a linear correction term to allow a better fit of the data. It is assumed in this modelling that the drop in shear stress right before the peak, due to the free state of the rotary column, does not influence the peak and subsequent weakening. All (a-b) values are negative, corresponding to the expected velocity weakening (table 6).

As mentioned before, the positive velocity dependence at 0.1 µms-1 may not be so large, and a foliation may not be present in all those experiments. Therefore the experiments may only in part represent a jump from a strengthening regime into a weakening regime.

The experiment jumping from 10µms-1 to 9.2 mms-1 does not show a peak at all, similar to our stepping experiments, which does not agree with RSF behaviour. Again, we cannot offer any explanation for this phenomenon.

5.4.2. Velocity jumps in room-dry halite plus muscovite gouges at high sliding velocities

The room-dry experiments in which velocity steps over the peak in strength were made first show a stage of hardening after the velocity change, before overcoming the peak strength. This is not a direct strengthening effect as described by RSF. After peak strength has been reached, rapid weakening to a very low coefficient of friction occurs in experiments with final velocities of 0.4 ms-1 and higher. The initial strengthening observed is not unique to our experiments. Recently Sone & Shimamoto (2009) simulated the waveform of the Chi-Chi earthquake rupture, in which slip is accelerated from 0 to 1.9 ms-1 in 6s and decelerated back in 4s, investigating its effect on the frictional strength of gouge. They also find a stage of initial strengthening, over displacements (termed 'characteristic strengthening distance' or Da) varying from 2-16 centimeters, before peak strength is reached and weakening starts to occur. As the slip rate decelerates, the fault gouge starts healing again. Da in our experiments ranges from ~0.2 m to 1.45 m. There seems to be an inverse relationship between the magnitude of the velocity change and this da value, but more data is necessary to prove this.

Despite the different accelerations, all experiments show strengthening, and we cannot but agree with Sone and Shimamoto (2009) that RSF indeed is not directly applicable to these high velocity experiments. The aforementioned authors suggest a modification the the RSF equation and add an initial strengthening term to account for the initial stage of strengthening. However, a physical basis for this is still lacking.

It is still unknown what causes this initial strengthening. Microstructural observations on HDR597 (0.01 – 0.22 ms-1) show similar microstructures as the pure halite sample deformed at a constant velocity of 0.1 ms-1. At 0.01 ms-1 deformation is expected to occur by cataclasis along a localized slip surface. As a jump in velocity is made, grainsize is reduced and healing can take place very fast, strengthening the material by forming the dense aggregates, as hypothesized before. After some time however, deformation does probably become localized causing the eventual weakening, as may be indicated by the very sharp slip surface at the top. This localization may somehow be promoted by temperature, as this is rising during strengthening. Some melt may have formed, but again we have no evidence for this.

5.5 Implications for natural fault zones

Halite provides a good analogue for studying brittle-ductile processes such as pressure solution and cataclasis at room temperature and low normal stresses. Plasticity does not become significant up to a normal load of 30 MPa (Shimamoto, 1986), or high temperatures. It is an anologue for quartzitic fault rock. Because phyllosilicates are ubiquitous in natural fault rock, we have added muscovite to the halite to improve the simulation of a real fault rock. Most of the presented experiments underwent large strains, and are representative of fault rock that have undergone large strains as well.

Room-dry and wet experiments have been conducted in this study, involving a broad range of slip rates and often very large shear strains. The room-dry experiments may be an analogue for quartzitic fault rock in which some solution -precipitation processes occur, but the extent of which may

be limited, and mechanical and thermal effects of pore fluids are absent. If similar processes and rates of healing are going on in natural rock, these results may form a unique demonstration of what happens in fault rock from very low to very high velocities. Results show a clear rate dependency of the measured friction coefficient; regimes of weakening & strengthening exist over the whole range of slip rates. Lower velocities need to be investigated to say more about the lowest velocity regime (whether it is stable or unstable). If our highest velocity experiments are representative of seismic deformation, we know that before the intense weakening found at these slip rates the gouges first strengthen again. Such strengthening may act as barriers to propagating earthquake rupture. Further studies connecting the analogue results to realistic deformation lows are required to extrapolate this data to nature. Thusfar we can only argue qualitatively.

The addition of muscovite creates an analogue with a quartzitic fault rock containing phyllosilicates. Results imply muscovite weakens the fault rocks at low velocities, and may inhibit healing to some extent as is argued by many other studies. However, the muscovite-halite relation may no longer be a realistic analogue, as the relative properties at high temperatures are much different for the quartz-halite system.

The wet results may form an analogue for a quartzitic fault rock containing phyllosilicates at hydrothermal conditions and low slip rates. At high slip rates it is no longer an analogue, as halite dissolves and the pore fluid evaporates.

Extrapolating our (wet) results to natural fault rock under hydrothermal conditions is hard, and microstructures form a crucial link in proving any relationship for this. In our wet experiments we have observed the early formation of muscovite-foliation, pressure solution effects, grain size reduction and fragmentation. We have to assume these are operating at similar rates, which is reasonable as observations on natural fault zones show similar microstructures, implying these processes are going on. Furthermore one needs to assume that the experimental geometry is not too simplistic to simulate natural fault zones, which are complex geometric structures.

This assumption brings us to the first important implication that our results have, namely that the effect of surface roughness of the wall-rock piston (which may be a laboratory analogue for the wall-rock surface in a natural fault) does have an effect on the sliding behaviour of the fault gouge. A smoother wall-rock is observed to yield a smaller dw and more unstable behaviour. Boldly stated, smoother faults in nature may be more unstable than are 'rougher' faults.

This study just scratches the surface as it comes to the complexity of an earthquake cycle. In the jumping experiments we try to simulate an earthquake by making a large velocity jump from a stably sliding fault gouge at much lower velocities. Of course this is just a simulation on simulated gouge. The maximum velocity jump was limited to 3 orders of magnitude. Deceleration was not studied, and experiments were conducted at room-dry conditions. Newer research makes use of a function generator steering the motor, in which a much more natural waveform can be loaded (eg. Togo et al., 2009). Still the experiments remain challenging; high-velocity experiments are difficult, and pore fluid pressures can still not be measured nor controlled, making it hard to do wet experiments.

We can only qualitatively speculate on the implications of our jumping data. The intermediate peak in strength may cause gradual initial strengthening, before weakening sets in. This may act as a barrier against propagating rupture, but we cannot quantify any of this. Future research should focus more on this transient part of fault behaviour and this initial strengthening portion, and pore fluids should be included as their influence may be significant. What we can say is that RSF is probably not directly applicable anymore at higher velocities.

6. Conclusions

Frictional sliding experiments were performed on analogue halite (+ muscovite) gouges in the HV2 rotary shear machine in Hiroshima University under low normal stresses, over a large range of slip rates and usually at very large shear strains. Experiments conducted at Utrecht University by Niemeijer & Spiers (2005) could be reproduced adequately in the HV2 machine. Dry gouge experiments were used to investigate the stability behaviour of the fault gouge from 0.1 μms-1 up to high slip rates of 1 ms-1. To study the effect of phyllosilicates, both pure halite gouge and halite gouge to which muscovite is added are investigated at dry conditions. Wet halite experiments were conducted to simulate processes operating near the brittle-ductile transitions and show a velocity strengthening region which forms an analogue to a creeping fault. Several velocity jumping (3 order magnitude velocity change) experiments were conducted from this strengthening region found in wet halite+ muscovite gouge, to simulate an earthquake rupture propagating upwards over a fault zone into a stably deforming region. Velocity jumps in dry halite-muscovite were conducted to study further the effect of a strengthening region on such a velocity change. Microstructures of various experiments were analyse to investigate the deformation process. Mechanical data and microstructural evidence indicate:

-There is a strong rate dependence in both dry and wet fault gouges.

-Some pressure solution is definitely occurring in the 'dry'experiments

-In the dry pure halite gouge we find 4 regimes of deformation. At the ultralow velocity regime (0.1-1 μms-1) pure halite exhibits some slip strengthening probably caused by healing effects by pressure solution leading to strengthening of the gouge and more distributed deformation. In the low velocity regime (1 μms-1 – 1(0) mms-1 strong slip weakening and velocity weakening occur, caused by localization and the accumulation of fine grained material along Y-shears. Healing of the fine-grained material causes stick-slip. The intermediate velocity regime (1(0) mms-1 – 0.1 ms -1) in the gouge shows velocity strengthening, which we propose is caused by an interplay of formation of dense aggregates by rapid healing process occurring in very fine material and the subsequent distributed fracturing of those aggregates. In the high velocity regime (>0.1 ms-1) strong velocity weakening occurs, which is probably caused by melt.

-The same 4 regimes are recognized for halite + muscovite. Overall muscovite causes a lower frictional strength at ultralow velocities, slip weakening instead of slip hardening at ultralow velocities and a bit more velocity strengthening at intermediate velocities. Muscovite inhibits pressure solution somewhat, presumably causing different healing rates.

-In the ultralow velocity regime the mixed gouge shows slip weakening and unstable behaviour, and is much weaker

than the pure halite gouge. The velocity dependence is uncertain in this region. This behaviour is explained by the formation of Y-shears and the accumulation of fine-grained material along these Y-shears prone to healing, causing stick-slip. In the low, intermediate and high velocity regime the mechanical data is similar to that of pure halite. Deformation in the low velocity regime is also by cataclasis and the formation of Y-shears. In the intermediate velocity regime muscovite containing gouge also strengthens, due to the interplay of formation of dense, strong aggregates by healing processes and the subsequent breaking up of those aggregates by distributed deformation. Muscovite may start to dehydrate, releasing water that promotes this healing, explaining why the mixed gouge is stronger than the pure gouge at these velocities. At high velocities very localized deformation takes place, and possibly some melting occurred.

-Different wall-rock pistons were investigated in wet gouge experiments. The surface roughness of the wall-rock piston influences the deformation behaviour, but not necessarily the steady state strength. The smoother the wall-rock, the shorter the characteristic weakening distance dw and the sooner the onset of stick-slip behaviour. Localization is inferred to occur faster in case of a smooth piston surface.

-The wet gouge shows behaviour as found in Niemeijer & Spiers (2005) with velocity strengthening below 1µms-1 and strong velocity weakening above 1 µms-1. The wet gouges were not suitable for high-velocity friction experiments. The early formation of a foliation is observed in the velocity strengthening region, implying frictional-viscous behaviour as described by Niemeijer & Spiers (2005) is occurring. Cataclasis, granular flow and some localization occur in the velocity weakening regime.

-Wet gouge at low slip rates behaves conform RSF when a large velocity step (jump) is made from the strengthening region at velocities < 1 µms-1. Stepping experiments above 1 µms-1 up to 1 mms-1 do not show typical RSF behaviour whilst this is expected, and no plausible explanation for this has yet been found.

-Experiments in dry halite + muscovite gouge investigated the influence of the velocity strengthening region found at intermediate velocities. When conducting a large velocity step from this regime into the high velocity weakening regime, an initial stage of slip hardening is observed. RSF is not (directly) applicable to these high-velocity experiments.

-The intermediate velocity strengthening may act as a barrier to earthquake rupture. More advanced experiments are required to investigate and identify the full scale of the complex processes going on during these high slip rates and construct constitutive equations that can be used in quantitative analysis and earthquake modelling.

References

Bos, B., & Spiers, C. (2001). Experimental investigation into the microstructural and mechanical evolution of phyllosilicate-bearing fault rock under conditions favouring pressure solution. Journal of Structural Geology 23 , 1187.

Bos, B., & Spiers, C. (2000). Fictional-viscous flow of phyllosilicate-bearing rock: Microphysical model and implications for crustal strength profiles. Journal of Geophysical Research Vol. 107 , B2,2028.

Bos, B., & Spiers, C. (2002a). Fluid-assisted healing processes in gouge-bearing faults: insights from experiments on a rock analogue systems. Pure and Applied Geophysics 159 , 2537-2566.

Bos, B., & Spiers, C. (2002b). Frictional-viscous flow of phyllosilicate-bearing fault rock: microphysical model and implications for crustal strength profiles. Journal of Geophysical Research 107 .

Brantut, N., Schubnel, A., Rouzaud, J.-N., Brunet, F., & Shimamoto, T. (2008). High-velocity frictional properties of a clay-bearing fault gouge and implications for earthquake mechanics. Journal of Geophysical Research Vol. 113 , B10401.

Carlslaw, H., & Jaeger, J. (1959). Conduction of heat in solids. Oxford University Press New York , 75.

Del Gaudio, P., Di Toro, G., Han, R., Hirose, T., Nielsen, S., Shimamoto, T., et al. (2009). Frictional melting of peridotite and seismic slip. Journal of Geophysical Research Volume 114 , B06306.

Di Toro, G., Hirose, T., Nielsen, S., Pennacchioni, G., & Shimamoto, T. (2006). Natural and experimental evidence of melt lubrication of faults during earthquakes. Science 311 , 647-649.

Dieterich, J. (1979). Modeling of rock friction 1. Experimental results and constitutive equations. Journal of Geophysical Research Vol. 84 , 2161-2168.

Dieterich, J., & Conrad, G. (1984). Effect of humidity on time- and velocity-dependent friction in rocks. Journal of Geophysical Research 89 , 4196-4202.

Digglen, E. v., Bresser, J. d., Peach, C., & Spiers, C. (2009). High shear strain behaviour of synthetic muscovite gouges under hydrothermal conditions. Journal of Structural Geology , 1-16.

Han, R., Hirose, T., & Shimamoto, T. (2010). Strong velocity weakening and powder lubrication of simulated carbonate faults at seismic slip rates. Journal of Geophysical Research Vol. 115 , B03412.

Hiraga, H., & Shimamoto, T. (1987). Textures of sheared halite and their implications for the seismogenic slip of deep faults. Tectonophysics 144 , 69-86.

Kawamoto, E., & Shimamoto, T. (1998). The strength profile for bimineralic shear zones: an insight from high-temperature shearing experiments on calcite-halite mixtures. Tectonophysics , 1-14.

Kiefer, S., Getting, I., & Kennedy, G. (1976). Experimental determination of the pressure dependence of the thermal diffusivity of Teflon, sodium chloride, quartz and silica. Journal of Geophysical Research Vol. 81, No. 71 , 3018-3024.

Kim, J.-W., Ree, J.-H., Han, R., & Shimamoto, T. (2010). Formation of pseudotachylite and mylonite in the brittle regime. submitted? in press?

Kim, J.-W., Ree, J.-H., Han, R., & Shimamoto, T. (2007). Frictional behavior and slip localization in simulated faults of halite at sub-seismic to seismic slip rates. Abstract Fall Meeting AGU .

Kitajima, H., Chester, F., & Chester, J. (2010). Dynamic weakening of fault gouge layers in high-speed shear experiments: Effects of thermal pressurization and temperature-dependent friction. Poster Earthscope Conference .

Mair, K., Renard, F., & Gundersen, O. (2006). Thermal imaging on simulated faults during frictional sliding. Geophysical Research Letters 33 , L19301.

Mariani, E., Brodie, K., & Rutter, E. (2006). Experimental deformation of muscovite shear zones at high temperatures under hydrothermal conditions and the strength of phyllosilicate-bearing faults in nature . Journal of Structural Geology 28 , 1569-1587.

Marone, C. (1998). Laboratory-derived friction laws and their application to seismic faulting. Annual Review Earth Planetary Science 26 , 643-696.

Marone, C. (1998). The effect of loading rate on static friction and the rate of fault healing during the earthquake cycle. Nature Vol. 391 , 69-72.

Mizoguchi, K., Hirose, T., Shimamoto, T., & Fukuyama, E. (2009). High-velocity frictional behavior and mincrostucture evolution of fault gouge obtained from Nojima fault, southwest Japan. Tectonophysics 471 , 285-296.

Morrow, C., Moore, D., & Lockner, D. (2000). The effect of mineral bond strength and adsorbed water on fault gouge frictional strength. Geophysical Research Letters Vol. 21 , 815-818.

Niemeijer, A., & Spiers, C. (2007). A microphysical model for strong velocity weakening in phyllosilicate-bearing fault gouges. Journal of Geophysical Research, Vol. 112 , B10405.

Niemeijer, A., & Spiers, C. (2005). Influence of phyllosilicates on fault strength in the brittle-ductile transition: insights from rock analogue experiments. In: Bruhn, D., Burlini, L. (Eds.), High-Strain Zones: Structure and Physical Properties. Special Publication. Geological Society of London, Nice , pp. 303-327.

Niemeijer, A., & Spiers, C. (2006). Velocity dependence of strength and healing behaviour in simulated phyllosilicate-bearing fault gouge. Tectonophysics 427 , 231-253.

Niemeijer, A., Marone, C., & Elsworth, D. (2010). Frictional strength and strain weakening in simulated fault gouge: competition between geometrical weakening and chemical strengthening. Journal of Geophysical Research Vol. 115 , B10207.

Niemeijer, A., Marone, C., & Elsworth, D. (2008). Healing of simulated fault gouges aided by pressure solution: Results from rock analogue experiments. Journal of Geophysical Research Vol. 113 , B04204.

Ohtomo, Y., & Shimamoto, T. (1994). Significance of thermal fracturing in the generation of fault gouge during rapid fault motion: An experimental verification (in Japanese with English abstract). Journal of the Tectonic Research Group of Japan 39 , 135-144.

Paterson, M., & Wong, T.-F. (2005). Experimental rock deformation: the brittle field. Springer-Verlag, Berlin .

Rice, J. (2006). Heating and weakening of faults during earthquake slip. Journal of Geophysical Research Vol. 111 , B05311-B05340.

Ruina, A. (1983). Slip instability and state variable friction laws. Journal of Geophysical Research, Vol. 88 , 10395-10370.

Scruggs, V., & Tullis, T. (1998). Correlation between velocity dependence of friction and strain localization in large displacement experiments on feldspar, muscovite and biotite gouge. Tectonophysics 295 , 15-40.

Shimamoto, T. (1989). The origin of S-C mylonites and a new fault zone model. Journal of Structural Geology Vol. 11 , 51-64.

Shimamoto, T., & Logan, J. (1986). Velocity-dependent behavior of simulated halite shear zones: an analog for silicates. Monogr. Am. Geophys. Union 37 , 49-63.

Sibson, R. (1973). Interactions between temperature and pore-fluid pressure during earthquake faulting and a mechanism for partial or total stress relief. Nature 243 , 66-68.

Sleep, N., & Blanpied, M. (1992). Creep, compaction and the weak rheology of major faults. Nature Vol. 359 , 687-692.

Sone, H., & Shimamoto, T. (2009). Frictional resistance of faults during accelerating and decelerating earthquake slip. Nature Geoscience Letters .

Tsutumi, A., & Shimamoto, T. (1996). Frictional properties of monzodiorite and gabbro during seismogenic fault motion. Journal of the Geological Society Japan Vol. 102 , 240-248.

Tsutumi, A., & Shimamoto, T. (19997). High-velocity frictional properties of gabbro. Geophysical Research Letters Vol. 24 , 699-702.

Wibberley, C., & Shimamoto, T. (2005). Earthquake slip weakening and asperities explained by thermal pressurization. Nature 436 , 689-692.

Zhang, S., Tullis, T., & Scruggs, V. (2001). Implications of permeability and its anisotropy in a mica gouge for pore pressures in fault zones. Tectonophysics 335 , 37-50.

Acknowledgements

I want to express my utmost gratitude towards my supervisor Prof. Dr. Chris Spiers, who is always an inspiring tutor and supported me through this entire project. I feel I have learnt an incredible amount over the past year. I am also extremely grateful towards my second supervisor Prof. Toshihiko Shimamoto, who made my visit to Japan possible, and who, despite his approaching retirement warmly welcomed me to Hiroshima University and with unstoppable energy tried to teach me as much as possible. I am thankful for his lectures on machines and fault behaviour, which gave me many new insights. I want to give warm thanks to Dr. Raehee Han, under whose careful guidance I conducted the first experiments of my life. Furthermore I want to thank Dr. Andre Niemeijer, who helped me when I was lost in the great amount of data I gathered in Japan, and who calculated the rate-and-state parameters for me. I want to thank Peter van Krieken for assisting with the thing sections and beautiful SEM photographs, which helped a great deal in understanding what was actually going on inside of the experiments. Last but not least, I want to thank all my friends and colleagues at 'Shimaken' from Hiroshima University and of the High Pressure Temperature laboratory in Utrecht for their interest, help and warm welcomes.